ALMA MATER STUDIORUM - UNIVERSITÀ DI BOLOGNA

SCUOLA DI INGEGNERIA E ARCHITETTURA

DICAM

SUSTEINABLE TECHNOLOGY AND BIOTECHNOLOGY FOR ENERGY AND MATERIALS

TESI DI LAUREA

in

Thermodynamics of Energy and Materials M

DEVELOPMENT AND CHARACTERIZATION OF CONDUCTIVE AND BIOCOMPATIBLE SCAFFOLDS FOR BIOMEDICAL APPLICATIONS

CANDIDATO   RELATORE:

Giovanni Mezzasalma   Chiar.mo Prof. Marco Giacinti Baschetti

CORRELATORI

Prof. Amparo Ribes Greus

PhD. Òscar Gil Castell

Anno Accademico 2017/18

Sessione II

Table of contents

Abstract

Nowadays, there is a growing demand of tissue engineered scaffolds for cell culture and subsequent tissue regeneration. In this line, biopolymers and biodegradable synthetic polymers have been proposed for fabrication of tissue engineered mats, which must mimic the intrinsic features of the natural extracellular matrix in terms of, among others, morphology, functionality, biocompatibility or degradability. Electrospinning is a popular technique to produce scaffolds that has the potential to address these issues.

In this work, a tailoring methodology was applied to obtain highly functionalized conductive polyester based scaffolds with high biocompatibility. For this purpose, blends based on polycaprolactone (PCL), gelatin (Ge) and polyaniline (PAni) were prepared into a hydrolytic solvent system and electrospun after several dissolution stages and times.

The obtained scaffolds were evaluated in terms of chemical composition, morphology and thermal properties. Regarding the biocompatibilization and the functionalization strategies, analyzing the scaffolds obtained after 24 h of dissolution time, it was found that the general characteristics, like the fiber diameter, thermo-oxidative stability and the thermal properties were influenced by the Ge concentration, while the PAni brought the electric conductivity to the nanofibers. On the other hand, for the tailoring strategy it was found that the dissolution time influenced the resultant physico-chemical properties and morphology of the electrospun scaffolds. Bead-free fibers were obtained after 24, 48 and 72 h of dissolution time, while some beads appeared after 96 h. The dissolution time influenced also the molar mass and the lamellar thickness of the electrospun scaffolds decreasing them, while increasing the crystallinity degree.

The preliminary *in vitro* validation revealed the release of the Ge fraction into the PBS solution and the consequent decrease of the initial mass of the nanofibrous scaffolds. In this line, future investigations for a deeper validation of the scaffolds may bring valuable information about their suitability in terms of *in vitro* biocompatibility and further *in vivo* implantation.

ii

Sommario

Attualmente, vi è una crescente domanda di scaffold per ingegneria tissutale per la coltura cellulare e la conseguente rigenerazione dei tessuti. In questa ottica, sono stati proposti biopolimeri e polimeri sintetici biodegradabili per la fabbricazione di scaffold, che devono imitare le caratteristiche intrinseche della naturale matrice extracellulare in termini, di morfologia, funzionalità, biocompatibilità o degradabilità. L'elettrofilatura (elettrospinning) è una tecnica popolare, per produrre scaffold, che ha il potenziale per risolvere questi problemi.

In questo lavoro, è stata applicata una metodologia di tailoring per ottenere scaffold conduttivi a base di poliestere con elevata biocompatibilità. A tale scopo, miscele a base di policaprolattone (PCL), gelatina (Ge) e polianilina (PAni) sono state preparate in un sistema solvente idrolitico ed elettrofilate dopo diverse fasi e tempi di dissoluzione.

Gli scaffold ottenuti sono stati valutati in termini di composizione chimica, morfologia e proprietà termiche. Riguardo alla biocompatibilità e alle strategie di funzionalizzazione, analizzando gli scaffold ottenuti dopo 24 ore di tempo di dissoluzione, si è riscontrato che le caratteristiche generali, come il diametro della fibra, la stabilità termo-ossidativa e le proprietà termiche erano influenzate dalla concentrazione Ge, mentre il PAni ha influenzato la conduttività elettrica delle nanofibre. D'altra parte, per la strategia di tailoring si è trovato che il tempo di dissoluzione influenzava le proprietà chimico-fisiche e la morfologia degli scaffold. fibre senza difetti (beads) sono state ottenute dopo 24, 48 e 72 ore di tempo di dissoluzione, mentre alcuni sono comparsi dopo 96 ore. Il tempo di dissoluzione ha influenzato anche la massa molare e lo spessore lamellare degli scaffold diminuendoli e aumentando il grado di cristallinità.

La validazione preliminare *in vitro* ha rivelato il rilascio della frazione di Ge nella soluzione di PBS e la conseguente diminuzione della massa iniziale degli scaffold nano-fibrosi. In questa linea, indagini future per una convalida più profonda degli scaffold potrebbero portare preziose informazioni sulla loro idoneità in termini di biocompatibilità *in vitro* e ulteriori impianti *in vivo*.

Resumen

Actualmente, existe una demanda creciente de scaffolds de ingeniería tisular para cultivo celular y posterior regeneración de tejido. En esta línea, se han propuesto biopolímeros y polímeros sintéticos biodegradables para la fabricación de scaffolds de ingeniería de tejidos, que deben imitar las características intrínsecas de la matriz extracelular natural en términos de, morfología, funcionalidad, biocompatibilidad o degradabilidad. Electrospinning es una técnica popular para producir scaffolds que tiene el potencial de abordar estos problemas.

En este trabajo, se aplicó una metodología de tailoring para obtener scaffolds conductivos basados en poliéster altamente funcionalizados con alta biocompatibilidad. Para este fin, se prepararon mezclas basadas en policaprolactona (PCL), gelatina (Ge) y polianilina (PAni) en un sistema de disolvente hidrolítico y se electrohilaron después de varias etapas y tiempos de disolución.

Los scaffolds obtenidos se evaluaron en términos de composición química, morfología y propiedades térmicas. En cuanto a las estrategias de biocompatibilización y funcionalización, al analizar los scaffolds obtenidos después de 24 h de tiempo de disolución, se encontró que las características generales, como el diámetro de la fibra, la estabilidad termo oxidativa y las propiedades térmicas se vieron influenciadas por la concentración de Ge, mientras que el PAni trajo la conductividad eléctrica a las nanofibras. Por otro lado, para la estrategia de tailoring se descubrió que el tiempo de disolución influía en las propiedades fisicoquímicas resultantes y en la morfología de los scaffolds electrohilados. Se obtuvieron fibras sin defectos (beads) después de 24, 48 y 72 h de tiempo de disolución, mientras que algunos aparecieron después de 96 h. El tiempo de disolución también influyó en la masa molar y el espesor laminar de los scaffolds disminuyéndolos, y aumentando el grado de cristalinidad.

La validación preliminar *in vitro* reveló la liberación de la fracción Ge en la solución de PBS y la consiguiente disminución de la masa inicial de los scaffolds. En esta línea, las investigaciones futuras para una validación más profunda de los scaffolds pueden aportar informaciones sobre su idoneidad en términos de biocompatibilidad in vitro y también implantación in vivo.

1 Motivation and aim

1.1 Motivation and overview

The failure of organ or tissue function as a result of injury, disease or aging has a high impact on quality of life and also incurs a large social and economic cost. Current treatments vary with the organ affected, but all of them have their limitations. Frequently, organ transplantation is the indicated therapy for these clinical cases; however, there are several disadvantages in using autologous or allogenic grafts, including shortage of appropriate donor organs, risk of disease transmission and immune rejection [1].

Tissue engineering (TE) is a promising approach for the repair of tissue defects that involves engineering and biological knowledge to create or restore tissue and organs. In general, tissue engineering is based in three main pillars: cells, biomaterials and biomolecules [2].

Cells in native tissue are surrounded by an extracellular matrix (ECM). Thus, mimicking the natural ECM structure has been considered as one of the main approaches to regenerate tissues. These artificial structures, known as scaffolds, should replicate the main features of natural ECM. An effective scaffold selected for tissue regeneration should provide suitable micro-environment for cell adhesion and proliferation. Properties such as the chemical composition, wettability, surface morphology, mechanical stiffness and elasticity will determine the cellular behavior during the *in vitro* cell culture and subsequent implantation *in vivo*. Various types of scaffolds have been proposed to meet the demand of tissue regeneration. Among them, nanofibrous scaffolds are widely used due to their high surface-area-to-volume ratio, high porosity, and interconnected pores which could facilitate cellular infiltration and transport of nutrition and waste [3].

In the past decades, electrospinning (ES) technology has been utilized to fabricate different fibrous scaffolds that imitate the microstructure of the natural ECM. ES is a simple and versatile technique that produces fibrous scaffolds in the nano-scale range, which offer a favorable micro-environment for cellular development by mimicking the native extracellular matrix [3]. This technique has gained popularity in the fabrication of nanofibrous scaffolds from several natural and synthetic materials, owning to its

simplicity and cost-effectiveness. The structure of electrospun nanofibers mimics the structure of native extracellular matrix (ECM), which is crucial for cell adhesion, spreading, and proliferation [4]. ES is an attractive approach for polymer biomaterials processing, providing an opportunity to control morphology, porosity and composition using relatively unsophisticated equipment. Nanofibers provide a connection between the nanoscale and the macroscale world. Although their diameters are in the nanometer range, they are very long entities, sometimes of the order of kilometers, which result in high flexibility and good mechanical performance. The possibility of design and produce scaffolds with controllable pore size, high porosity with interconnected pores and permeability, as well as good biocompatibility and cell affinity, make the scaffolds of polymer nanofibers effective candidates for TE applications [5]. Electrospun nanofibers scaffolds can also be tailored in accordance with the purpose of their use [6].

The importance of electrospun nanofiber in the biomedical field can be determined from the fact that numerous articles are being published on a regular basis highlighting its importance in the biomedical engineering field, using biocompatible and biodegradable (natural or synthetic) polymers. However, several synthetic biocompatible polymers used in tissue engineering, such as the polycaprolactone (PCL), lack bioactive sites for further bio-functionalization. Nowadays the researchers have shown that hybrid natural and synthetic polymer blends could better support cell adhesion and proliferation and be potential candidates for surface endothelialization. Among natural polymers, gelatin, which is derived from the partial hydrolysis of native collagen with its relatively low molecular weight, promotes an easy and stable electrospinning process. Furthermore, it contains many integrin binding sites for cell adhesion, migration, and differentiation. As suggested in the literature, the combination of gelatin and PCL is an efficient approach to overcome their individual shortcomings, showing potential to be used as tissue constructions [7]. Up to now, some biocompatible synthetic polymers, such as PCL, have been used to fabricated artificial vascular systems. PCL exhibits good biocompatible, biodegradable and mechanical properties, moreover hydrolysis of PCL does not produce a local acidic environment which could compromise cell growth [8].

On the other hand, conducting fibers have received a great deal of attention, because their morphology, able to mimic the natural ECM structure for tissue engineering, is coupled

with the possibility to provide electrical stimulation or electroactivity of substances, which can significantly influence the cellular attachment, proliferation, differentiation and regeneration or tissue repair [9]. Among conducting polymers, the polyaniline (PAni) can be considered as a potential prospective candidate for tissue engineering and regenerative medicine, in part due to its excellent electrical conductivity, good redox stability, reversible oxidation, and biocompatibility [10]. PAni has also been proven to stimulate cells attachment, proliferation, migration, and differentiation through a modulation electrical stimulus [11]. However, pure PAni exhibit brittleness and poor mechanical properties. Therefore, developing flexible conductive PAni scaffolds with satisfying mechanical properties has obtained particular attention in tissue engineering. Blending PAni with biocompatible synthetic polymers is necessary to fabricate flexible conducting materials for tissue engineering. As reported in [3] the use of PAni could enhance the *in vitro* attachment, spreading and survival of Human umbilical vein endothelial cells (HUVECs) under electrical stimulation.

1.2 Aim

With the aim of improving mechanical properties, electrical conductivity and biocompatibility of the scaffolds used in tissue engineering, this master thesis focuses on the production and characterization of nanofibrous electrospun scaffolds. The research approach in this work is based on the preparation, characterization and preliminary validation of polymeric blends, based on polycaprolactone (PCL) and gelatin (Ge) with the incorporation of polyaniline (PAni). For this purpose, an electrospinning setup and a hydrolytic assisted process are used to obtain the functionalized scaffolds.

This general objective will be achieved through the following partial objectives:

- Prepare blends of PCL/Ge/PAni dissolve them into1:1 formic/acetic acid solvent.
- Optimize the process of obtaining nanofibrous scaffolds through the electrospinning.
- Characterize the nanofibrous scaffolds in terms of morphology, chemical composition, conductivity and thermal properties.
- Evaluate the influence of the Ge concentration as biocompatibilization strategy.

- Assess the influence of the PAni concentration as conductive functionalization approach.
- Analyze the influence of the dissolution time as tailoring strategy purpose.
- Preliminary validate the behavior of the scaffolds in simulated physiologic conditions.

2 Tissue engineering

Tissue engineering is a multidisciplinary field that combines the principles of engineering and life sciences for the development of biological substitutes for restoration, maintenance, or improvement of tissue function. Biomaterials research is an emerging field which plays a pivotal role in tissue engineering by serving as matrices for cellular in growth, proliferation, and new tissue formation in three-dimensions. As an interdisciplinary technique, TE uses three basic components to develop bio-functional substitutes for restore and maintenance of tissue function: cells, biomaterials and biomolecules. Tissue engineering involves the treatment of dissimilar tissues such as skin, bone, nerve, cardiac [12].

2.1 Scaffolds in tissue engineering

The application of biomaterials in TE is predominately in the form of scaffolds that act as the temporal shape or physical guidance of the tissue to be regenerated. However, it is still a big challenge to design an ideal scaffold that mimics the structure and biofunctions of the native ECM. A good scaffold for TE applications should [13]:

  i.   provide a physical environment and bioactive stimuli that support the cell biofunctionality and tissue formation;
  ii. give mechanical strength similar to the tissue it replaces;
  iii. act as a reservoir of soluble factors which include growth factors;
  iv. allow remodeling by cells to restore the tissue architecture.

Electrospun nanofibers, due to their porous structure and high surface-area-to-volume ratio, have shown to favor the adhesion, proliferation and differentiation of various cells, and serve as promising structures for tissue regeneration [14]. It is reported that the properties of electrospun nanofibers such as the chemical composition, fiber diameter and orientation could affect the proliferation, morphology and differentiation of cells [15].

While the composition and surface chemistry of the scaffolds dictate the ability of cells to initially attach, the morphology of the scaffold plays a key role in controlling their ability to migrate. Besides allowing cell penetration, a proper architecture of the scaffold will allow nutrients and oxygen to flow into it, as well as to remove waste produced by

the cells to increase cell survival and hence to regenerate tissue. Thus, scaffolds need to be designed to present enough porosity, which not only has to have pores big enough to allocate cells, but also needs to present interconnections to allow cell migration between the different pores. Porosity is the quantification of void spaces within a material [16]. The optimum pore size for scaffolds lies in the range between 100 and 400 μm. Nevertheless, the pores not only play a significant role in allowing cell penetration and migration, but also significantly influence the physical properties of the scaffold. For instance, porosity increase is known to exponentially decrease the mechanical properties of the materials, whereas it can largely increase the permeability [17]. In order to optimize scaffolds for TE, therefore, all these parameters need to be balanced to guide proper tissue regeneration. The total porosity, the pore size and pore size distribution as well as the pore morphology are some key parameters that play a critical role in balancing the physical and biological properties of the scaffolds. Furthermore, these properties need to be balanced with the degradation of the scaffold, that should be as fast as the formation of new natural tissue, which is stimulated by the biomaterial. In this concern, high porosity is also known to increase the ability of fluids to penetrate the structure and therefore enhances the degradation [18].

ES technique has greatly accelerated the development of innovative grafting scaffolds for tissue engineering. Various natural and synthetic polymers have been electrospun into nanofibrous scaffolds for TE. Natural polymers, such as collagen, gelatin, silk, chitosan and fibrinogen, have been fabricated into nanofibers for wound healing, and cell culture results showed that those fibers could favor the attachment and proliferation of keratinocytes or fibroblasts [19]. On the other hand, multiple biodegradable synthetic polymers, including PGA, PLA, PCL and their copolymers, are commonly used for TE applications because of their favorable mechanical and biodegradable properties [20]. However, the hydrophobic surface and the lack of cell-recognition signals limit their application for the production of scaffolds. Recently, more researches are focusing on the production of nanofibrous scaffolds using blends that possess both the physical properties of synthetic polymers and bioactivity of natural polymers [21], [22].The electrospun scaffolds have proven to be applicable on several TE application; examples of biomedical applications could be: skin recovery, nerve regeneration, bone and cardiac bioengineering.

6

For wound healing application, the high porosity of electrospun nanofibers could provide more structural space for accommodation of the grafted cells, facilitate cell proliferation and migration and improve oxygen exchange, nutrient delivery and exudates elimination. One the other hand, the small pore size of nanofibrous scaffolds is able to limit wound infection and dehydration during wound healing. Additionally, the tunable mechanical properties of electrospun nanofibers could retain mechanical integrity between TE grafts and host tissue, and also prevent wound contraction during implanting [23].

Unlike soft tissues in our body, bone is a physically hard, rigid and strong connective tissue, which microscopically contains relatively small number of cells within abundant ECM in the form of collagen nanofibers and stiffening inorganic substrate, such as hydroxyapatite (HA). Therefore, the unique bone ECM is an organic-inorganic nanofibrous composite, in which osteocytes are able to perform good functions and biological roles. To develop bone ECM mimicking scaffolds, electrospun composite nanofibers of degradable polymers and calcium phosphate are subject of substantial investigations for bone TE [12], [24].

Other interesting application of electrospun nanofibers is for nerve regeneration. The aim of nerve TE is to develop effective neural guidance conduits for bridging gaps in damaged peripheral or central neurons, and the function of neural TE scaffolds should be directing axonal sprouting and promoting the diffusion of neurotrophic factors [25]. Electrospun nanofibers are suitable materials for nerve TE as their structure not only mimics the neural fibrous ECM, but also provides substrate topographical guidance to direct neural cells growth [26]. Recently, the application of electrical stimulation in nerve TE has become an emerging approach to promote neurite growth and neural differentiation, and electrically conductive nanofibers have been developed as a crucial substrate for electrical stimulation. Therefore, conductive polymers have been incorporated into nanofibers during ES [27].

In addition, cardiac TE gained great attention recently as it promises to revolutionize the treatment of patients with end-stage heart failure and provide new solutions to the serious problems of heart donor shortage [28]. Electrospun nanofibers have been considered high-attentive scaffolds for cardiac TE because their tunable mechanical properties and orientation of fibers are significant for myocardial regeneration [29].

2.2   Polymers for tissue engineering applications

There is a wide range of polymers used for the development of nanofibrous scaffolds for tissue engineering applications. Over the last years, more than 200 polymers have been successfully electrospun from several natural and synthetic polymers and characterized with respect to their applications [30].

Natural polymers exhibit high biocompatibility and low immunogenicity, compared to the synthetic ones, when used in biomedical applications. A strong reason for using natural polymers for TE is their inherent capacity for binding cells since they carry specific protein sequences, such as RGD (arginine/glycine/aspartic acid). Typical natural polymers include collagen, chitosan, gelatin, casein, cellulose acetate, silk protein, chitin, fibrinogen, etc. Scaffolds fabricated from natural polymers promise good clinical functionality [31]. However, low mechanical and hydrolytic stability as well as partial denaturation of natural polymers has been reported [32].

Synthetic polymers often offer many advantages over natural polymers as they can be tailored to give a wider range of properties, such as necessary mechanical properties and desired degradation rate [33]. Typical synthetic polymers used in biomedical applications are hydrophobic biodegradable polyesters, such as polyglycolide (PGA), polylactide (PLA), the copolymer poly(lactide-co-glycolide) (PLGA) and poly (ε-caprolactone) (PCL), which have all been electrospun into nanofibrous scaffolds for bone TE, cardiac grafts, wound dressings and for engineering of blood vessel substitutes [30].

An ideal scaffold should have the architecture, mechanical and biological features that are similar to the native tissue. For this reason, the selection of appropriate biomaterials is critical in order to produce a scaffold that recapitulates the architecture and functionality of the native tissue ECM. Biocompatibility is one of the most important requirements when selecting the right biomaterials for scaffold fabrication. Recently, literature proposed that hybrid natural and synthetic polymer blends could better support cell adhesion and proliferation, and be potential candidates for surface endothelialization [7], [13].

Among the several polymers used for the production of scaffold for TE applications, in this study are used blends of polycaprolactone (PCL), gelatin (Ge) and polyaniline

(PAni). Concretely, the development of functionalized scaffolds based on PCL and Ge have shown promising results [34]. Moreover, the introduction of conductive polymers such as the PAni would bring new possibilities in the field of stimuli required for tissue engineering applications [35].

2.2.1 *Polycaprolactone (PCL)*

The polycaprolactone (PCL) is a semi-crystalline, biodegradable hydrophobic polyester showing a glass transition temperature (T_g) of -60 °C and melting point ranging between 59 and 64 °C. It is characterized by offering high plasticity, ductility and a slow degradation rate resulting from the hydrolysis of its ester linkages. It is soluble in chloroform, dichloromethane, carbon tetrachloride, benzene, toluene, cyclohexanone and 2-nitropropane at room temperature. It has a low solubility in acetone, 2-butanone, ethyl acetate, dimethylformamide and acetonitrile and is insoluble in alcohol, petroleum ether and diethyl ether [34]. The molecular structure of the PCL is shown in Fig. 1.

Given the biodegradability of the PCL in physiological conditions and the lack of inflammatory compounds during the degradation, it has been proposed as an implantable biomaterial for tissue engineering applications. Specifically, the low degradation rate of the PCL, promoted its use for the preparation of long-term implants and controlled drug release applications. However, when it comes to short-term TE applications, the slow degradation rate may result in a drawback. This is the reason why the PCL is usually modified by means of copolymerization or blending, among other strategies in order to better control their properties and fit the degradation rate for the given purpose [3], [36], [37].
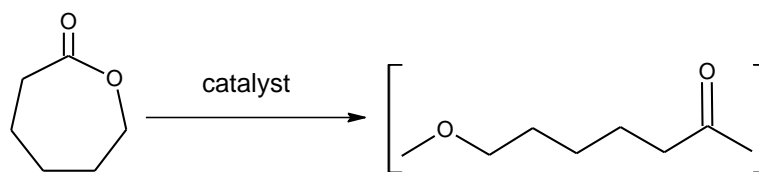

Fig. 1 Molecular structure of ε-caprolactone and PCL [37].

2.2.2 *Gelatin*

The molecular structure of Gelatin (Ge) is shown in Fig. 2; it is a natural polymer derived from collagen by controlled hydrolysis, commonly used for pharmaceutical and medical applications because of its high biodegradability and biocompatibility in physiological conditions. Generally, gelatin can be classified as Type A and Type B depending on the hydrolysis condition of isolation from collagen [38].

Gelatin is rarely considered as solely candidate material for TE applications, due to its high solubility in water in its natural state and poor mechanical stability. Accordingly, gelatin has been satisfactorily combined with other polymers by blending strategies for the preparation of TE scaffolds [30].
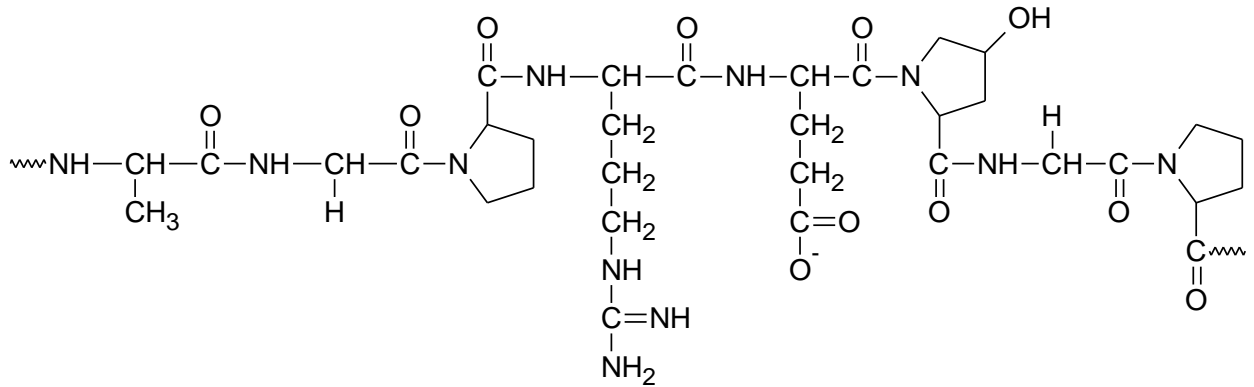

Fig. 2 Basic molecular structure of gelatin [39].

2.2.3 *Polyaniline*

Polyaniline (PAni) is a multifunctional conductive polymer with potentials for biomedical applications, combining electrical conductivity, free radical-scavenging capacity, antimicrobial activity and biocompatibility [40]. The PAni has been investigated due to its unique proton dopability, excellent redox recyclability, chemical stability, variable electrical conductivity (which can be varied by changing the pH at which it is prepared), low cost and ease of synthesis. The molecular structure of the PAni is shown in Fig. 3.

Recent studies revealed that electrospun fibers containing PAni are suitable substrates for cell culture and TE. The electrical stimulation ability of these electrospun fibers, can enhance cell differentiation for neurons, cardiomyocytes and myoblasts. Moreover, the antimicrobial properties against different bacteria of PAni can be beneficial for some in biomedical applications. The ability to inhibit bacterial growth has significant advantages to the wound-healing process and antimicrobial materials are potentially suited for wound-dressing applications [41].
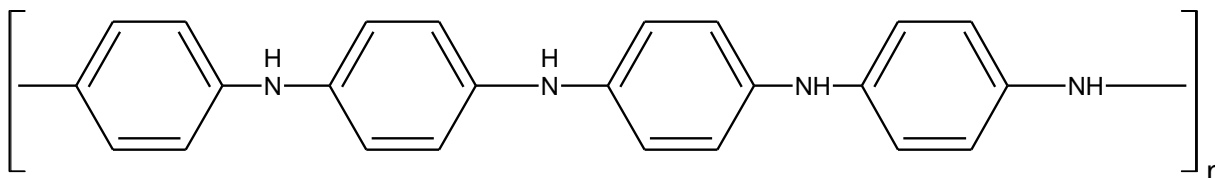
Fig. 3 Molecular structure of PAni [40].

2.3 Obtaining of scaffolds for tissue engineering: electrospinning

Most of the scaffolds were conventionally developed with an objective of drug delivery but later explored for 3D cell culture in the context of tissue engineering. Some of these conventional processing techniques for scaffold fabrication are: extrusion or melt molding using blowing agents; Compression molding with particle leaching; Injection molding and 3D printing [42].

The promising techniques of modern age are Electrospinning, CAD based 3D plotting and self-assembling peptides. Each technique helps in fabricating scaffolds with varied pore size, shape and structure. 3D plotting is a method adapted from mechanical engineering disciplines. With this technique the scaffold is created layer by layer, allowing the fabrication of very complex architectures [43]. Self-assembling peptides are the new age designed biomaterials that offer molecular level control over the scaffolds. Additionally, they can be used for in situ assembly through injection mode, if appropriately designed [44]. Unlike synthetic polymers, designed peptides are much closer to natural ECM and can be manipulated by using chiral amino acids to achieve desired topological features in the scaffold [45].

In the last decade electrospinning gained increasing interest as a potential polymer processing technique for applications in tissue engineering, thanks to its relative ease of use, adaptability, and the ability to fabricate fibers with diameters on the nanometer size scale. This technique is preferred over other processing methods because of the small diameter of the produced nanofibers that mimic the ECM and possess a high surface area to volume ratio. All these features can enhance cell attachment, drug loading and mass transfer properties and also affords the opportunity to engineer scaffolds with tailored morphology and further application behavior.

There are basically three components to complete a functional ES set-up: a high voltage power supply, a spinneret constituted by a glass capillary tube or a needle of small diameter, and a grounded metal collecting screen, as shown in Fig. 4. The ES apparatus is usually set up in a chemical hood to allow the exhaustion of organic vapors. In addition, a closed, non-conductive environment, often with temperature and humidity control, is required to avoid interference from environmental factors, such as air turbulence.

In some cases, the capillary is placed perpendicularly to the collection surface, letting the polymer fluid drop under gravity and placing the collector underneath. Occasionally the capillary can be tilted at a defined angle to control the flowrate through the capillary. However, in the most frequent setup, the capillary is mounted horizontally, and a pump is used to initiate the droplet. The pump can be also used in the case of vertical feeding. The electrode can be inserted either in the polymer fluid or placed onto the tip of the capillary if a syringe with a metal needle is used. The collector is usually a plane metal sheet or a grid that can be covered with a fabric (Fig. 4 a), although other collectors such as rotating cylinders covered with a grounded aluminum sheet could also be used [5] (Fig. 4 b).
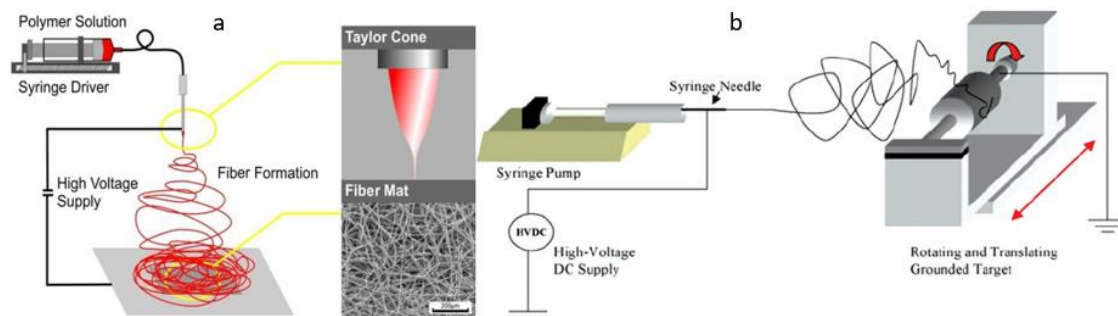
Fig. 4 *Schematic representation of a vertical (a) and a horizontal (b) ES apparatus with a plane metal sheet collector and a rotating cylinder collector, respectively* [5], [12].

The ES process begins when electric charges move into the polymer solution via the metallic needle. This causes instability within the polymer solution due to the induction of charges on the polymer droplet. At the same time, the reciprocal repulsion of charges produces a force that opposes the surface tension, and ultimately the polymer solution flows in the direction of the electric field, as shown in Fig. 5. A further increase in the electric field causes the spherical droplet to deform and assume a conical shape. At this stage, ultrafine nanofibers emerge from the conical polymer droplet, the so-called Taylor

cone (Fig. 5f), which are collected on the metallic collector kept at an optimized distance. A stable charged jet can be formed only when the polymer solution has sufficient cohesive force. During the process, the internal and external charge forces cause the whipping of the liquid jet in the direction of the collector. This whipping motion allows the polymer chains within the solution to stretch and slide past each other, which results in the creation of fibers with diameters small enough to be called nanofiber [6].
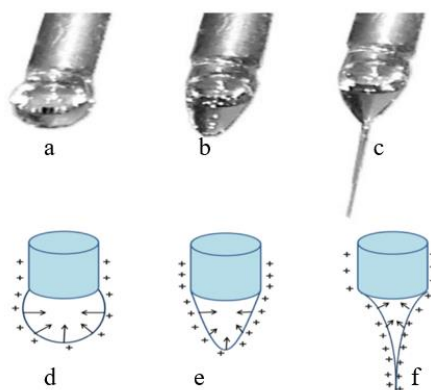
Fig. 5 From a to c: three-stage deformation of the polyvinylpyrrolidone droplet under the influence of increasing electric field. From d to f: mechanism of the effect of charges on the polymeric droplets [6].

There are several factors that affect the ES process, which are classified as processing, solution and environmental parameters. The processing parameters include the applied electric field, the distance between the needle and collector, the flow rate, and the needle diameter. The solution parameters include the solvent, polymer concentration, viscosity and solution conductivity. The environmental parameters include relative humidity and temperature. All these parameters directly affect the generation of smooth and bead-free electrospun fibers. Therefore, to gain a better understanding of the ES technique and fabrication of polymeric nanofibers, it is essential to thoroughly understand the effects of all of these governing parameters [6].

2.3.1 *Processing parameters*

Voltage

The strength of the applied electric field controls the formation of fibers from several microns in diameter to tens of nanometers. Suboptimal field strength could lead to bead defects in the spun fibers or even failure in jet formation. Generally, it is known that the

current flow from a high-voltage power supply into a solution via a metallic needle will cause a spherical droplet to deform into a Taylor cone and form ultrafine nanofibers at a critical voltage (Fig. 5 d-f and Fig. 6 a-d). At low voltages, a pendant drop is formed at the tip of the capillary (a). The Taylor cone (dark gray) then forms at the tip of the pendant drop. However, as the applied voltage is increased the volume of the pendant drop decreases until the Taylor cone is formed at the tip of the capillary (c). Increasing the applied voltage further results in the fiber jet being ejected from within the capillary (d), which is associated with an increase in bead defects.
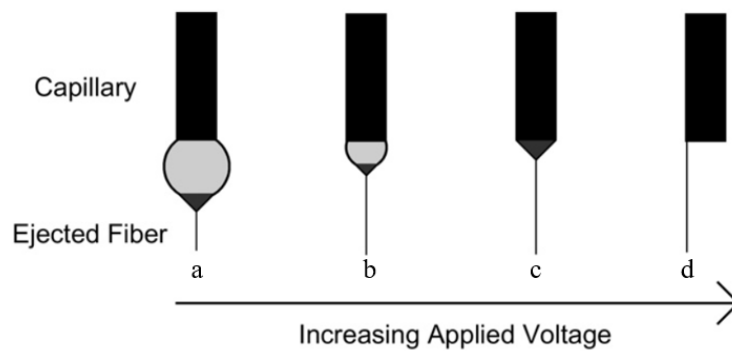
Fig. 6 Effect of the variation of the applied voltage on the formation of the Taylor cone [12].

The critical value of applied voltage varies from polymer to polymer. The formation of smaller-diameter nanofibers with an increase in the applied voltage is attributed to the stretching of the polymer solution in correlation with the charge repulsion within the polymer jet. An increase in the applied voltage beyond the critical value will result in the formation of beads or beaded nanofibers. The increases in the diameter and formation of beads or beaded nanofibers with an increase in the applied voltage are attributed to the decrease in the size of the Taylor cone and increase in the jet velocity for the same flow rate [6].

Flow rate

The flow of the polymeric solution through the metallic needle tip may determine the morphology of the electrospun nanofibers. Uniform bead-less electrospun nanofibers could be prepared via a critical flow rate for a polymeric solution. This critical value varies with the polymer system. Increasing the flow rate beyond a critical value not only leads to increase in the pore size and fiber diameter but also to bead formation due to

incomplete drying of the nanofiber jet during the flight between the needle tip and metallic collector [5]. In this sense, a minimum flow rate is preferred to maintain a balance between the leaving polymeric solution and replacement of that solution with a new one during jet formation. This will also allow the formation of a stable jet cone (Fig.7 a) even if sometimes it can cause the formation of a receded jet that emerges directly from the inside of the needle with no apparent droplet or cone. Receded jets are not stable jets, and during the ES process, these jets are continuously replaced by cone jets. As a result of this phenomenon, nanofibers with a wide range diameter are formed.

In addition to bead formation, other defect that have also been reported, usually associated with elevated flow rate, are ribbon-like defects and unspun droplets. Their formation is mainly attributed to the uncomplete evaporation of the solvent and low stretching of the solution in the flight between the needle and metallic collector [6].
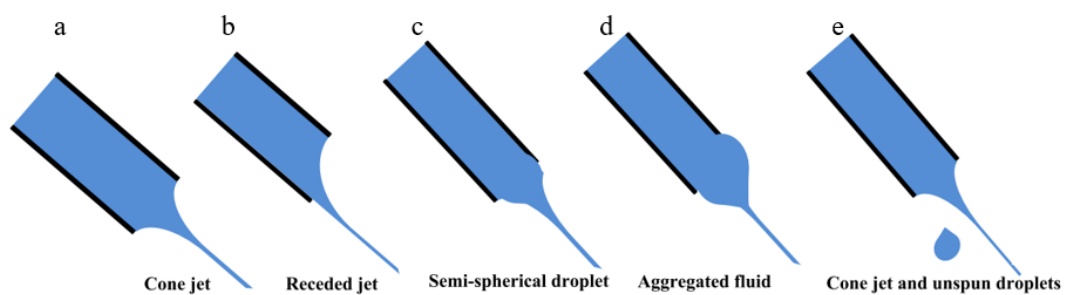
Fig. 7 Formation of various jets with increasing flow rate [6].

Needle tip to collector distance

The distance between the metallic needle tip and collector plays an essential role in determining the morphology of an electrospun nanofiber. The nanofiber morphology could be easily affected by the tip-to-collector distance, since it will determine the deposition time, evaporation rate, and whipping or instability interval. Hence, a critical distance needs to be maintained to prepare smooth and uniform electrospun nanofibers, and any changes on either side of the critical distance will affect the morphology of the nanofibers. Numerous research groups have studied the effect of the distance between the needle tip and collector and concluded that defective and large-diameter nanofibers are formed when this distance is kept small, whereas the diameter of the nanofiber decreased as the distance was increased [6].

2.3.2 *Solution parameters*

Polymer concentration and solution viscosity

As commented before, the ES process relies on the phenomenon of the uniaxial stretching of a charged jet. The stretching of the charged jet is significantly affected by changing the concentration of the polymeric solution, which determines the average fiber diameter, as shown in Fig. 8.
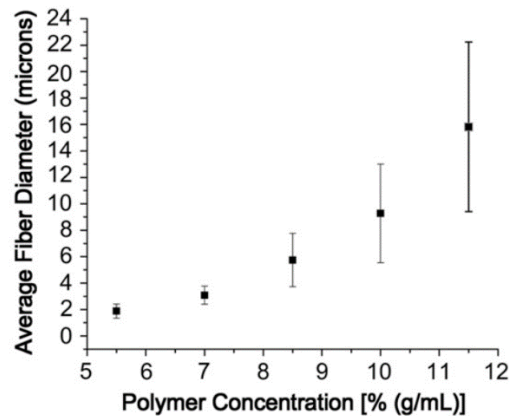

Fig. 8 Effect of polymer concentration on fiber diameter [12].

When the concentration of the polymeric solution is too low, the applied electric field and surface tension cause the entangled polymer chains to break into fragments before reaching the collector. These fragments cause the formation of beads or beaded nanofibers. Increasing the concentration of the polymeric solution will lead to an increase in the viscosity, which then increases the chain entanglement among the polymer chains. These chain entanglements overcome the surface tension and ultimately result in uniform bead-less electrospun nanofibers. on the other hand, further increase of the concentration, beyond a critical value, may obstruct the flow of the solution through the needle tip, due to the polymer solution drying, which ultimately results in defective nanofiber. The morphologies of the beads depict an interesting shape change from a round droplet-like shape –with low-viscosity solutions– to a stretched droplet or ellipse to smooth fibers – with sufficient viscosity– as the solution viscosity changes (Fig. 9 a-d). Hence, it can be concluded that in addition to the ES parameters, the determination of the critical value of the concentration/viscosity is also essential to obtain bead-less nanofibers [6], [46].
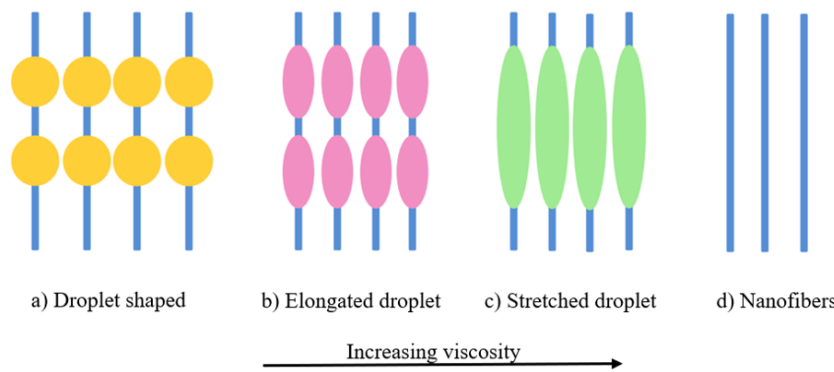
a) Droplet shaped   b) Elongated droplet   c) Stretched droplet   d) Nanofibers

Increasing viscosity

Fig. 9 Schematic variation in morphology of electrospun nanofibers with viscosity [6].

Polymer molar mass

The molar mass of the polymer has a significant effect on the rheological and electrical properties such as the viscosity, the surface tension, the conductivity and the dielectric strength. This parameter affects the morphology of electrospun fiber.

Generally high molar mass polymer solutions have been used in ES as they provide the desired viscosity for the fiber generation. It has been observed that a low molar mass polymer solution tends to form beads rather than fibers and a high molar mass solution gives fibers with larger average diameters. Molar mass of the polymer reflects the entanglement capability of the polymer chains in a solution, thus solution viscosity. Hence, even when polymer concentration is low, high molar mass polymers can maintain enough number of entanglements of the polymer chains, thus ensuring a sufficient level of solution viscosity to produce a uniform jet during ES and restrain effects of surface tension, which plays a significant role in beads formation on electrospun nanofibers [30].

Solution conductivity

The solution conductivity strongly influences the Taylor cone formation, the stability of the electrospinning process and subsequently the morphology and diameter of the nanofibers. In a solution with low conductivity, the surface of the droplet will have not enough charge to form a Taylor cone and ES will not take place. Increasing the conductivity of the solution to a critical value will increase the charge on the surface of the droplet to form Taylor cone and result into a decrease in the fiber diameter. Increasing the conductivity beyond a critical value will again hinder the Taylor cone formation and subsequently suitable ES. This phenomenon could be explained by taking into

consideration the entire ES process. The ES process is dependent on the Coulomb force between the charges on the surface of the fluid and the force due to the external electric field. However, the formation of the Taylor cone is governed largely by the electrostatic force of the surface charges created by the applied external electric field. An ideal dielectric polymer solution will not have enough charges in the solution to move onto the surface of the fluid; hence, the electrostatic force generated by the applied electric field will not be sufficient to form a Taylor cone and initiate ES process. In contrast, a conductive polymer solution will have sufficient free charges to move onto the surface of the fluid and form a Taylor cone and initiate the ES process. The conductivity of a polymer solution could be controlled by the addition of an appropriate additive to the solution such as salt, as it increases the number of ions in the polymer solution, which results in the increase of surface charge density of the fluid and the electrostatic force generated by the applied electric field [6].

Solvent type

A solvent performs two crucial roles in ES: firstly, to dissolve the polymer molecules for forming the electrified jet and secondly to carry the dissolved polymer molecules towards the collector. For this reason, the selection of the solvent is one of the key factors for the formation of smooth and bead-less electrospun nanofibers. Usually, the selection of the solvent relies in two main factors: solubility, boiling point and surface tension. First, the preferred solvents for ES process are those that completely solubilize the polymer. Second, the solvent should have a moderate boiling point, which is strictly correlated to the volatility of the solvent. Generally, volatile solvents are preferred as their high evaporation rates encourage the easy evaporation of the solvent from the nanofibers during their flight from the needle tip to collector. However, highly volatile solvents are mostly avoided because their low boiling points and high evaporation rates cause the drying of the jet at the needle tip, which will hinder the ES process. Similarly, less volatile solvents are also avoided because their high boiling points prevent their drying during the nanofiber jet flight. The deposition of solvent-containing nanofibers on the collector will cause the formation of beaded nanofibers.

It is well known that the morphology and size of electrospun nanofibers strongly depend on the solution properties such as the surface tension. Different solvents may contribute

to dissimilar surface tensions. Moreover, the surface tension depends on both the polymer and solvent. By reducing the surface tension of a polymer solution, fibers could be obtained without beads. However, an extremely low surface tension is not always suitable for ES as fiber could be easily broken in small droplets causing an electrospraying rather than an electrospinning.

Tab. 1 gathers some of the characteristic values for the traditionally used solvents such as the surface tension, the dielectric constant and the boiling point, which should be kept in mind during selection for ES process. Nevertheless, several alternative solvents have been recently proposed for the electrospinning of PCL, with the aim of reducing the exposure of technicians to toxic solvents and tailoring the physico-chemical properties and morphology of the electrospun fibers [30].

Tab. 1 Properties of different solvents used in electrospinning process [30].

Solvents	Surface tension (mN·m⁻¹)	Dielectric constant	Boiling point (°C)	Density (g·ml⁻¹)
Chloroform	26.5	4.8	61.6	1.498
Dimethylformamide (DMF)	37.1	38.3	153	0.994
Hexafluoroisopropanol (HFIP)	16.1	16.7	58.2	1.596
Tetrahydrofuran (THF)	26.4	7.5	66	0.886
Trifluoroethanol (TFE)	21.1	27	78	1.393
Acetone	25.2	21	56.1	0.786
Water	72.8	80	100	1.000
Methanol	22.3	33	64.5	0.791
Acetic acid	26.9	6.2	118.1	1.049
Formic acid	37	58	199	1.21
Dichloromethane	27.2	9.1	40	1.326
Ethanol	21.9	24	78.3	0.789
Trifluoroacetic acid	13.5	8.4	72.4	1.525

Dissolution time

As introduced in the previous section, novel alternative solvents have been proposed with the purpose of avoiding toxicity, being more sustainable and economically affordable. Such is the case of the acetic and formic acid, ethanol or acetone. Nevertheless, the use

of these solvents is usually conditioned by different circumstances, as the hydrolytic degradation of labile bonds, the use of specific additives to improve spinnability, etc.

The use of the novel alternative solvents such as the formic/acetic acid mixture for the PCL may induce hydrolytic degradation of the ester bonds which becomes more pronounced when high dissolution time is considered [47]. Although hydrolytic degradation of PCL occurs in an aqueous acidic media, it was shown that the viscosity of a PCL solution in formic/acetic acid was high enough for suitable ES in steady-state conditions [48]. However, the hydrolytic degradation during dissolution can be virtuously considered for systematically tuning of the molar mass of the polymer and thus, many other parameters correlated such as the solution viscosity and physico-chemical features of the nanofibers. Among them, the fiber diameter, the polymer crystallinity, lamellar thickness or hydrophilicity may be also tailored by properly adjusting the dissolution time [48].

2.3.3 *Ambient parameters*

Beside the processing and solution parameters, the environmental or ambient factors such as relative humidity and temperature may also affect the diameter and morphology of the nanofibers.

Humidity

Humidity cause changes in the nanofibers diameter by controlling the solidification process of the charged jet. This phenomenon is, however, dependent on the chemical nature of the polymer. High humidity lead to the formation of pores in the fibers. Too low humidity would result in higher evaporation of volatile solvents that can produce the blockage of the needle.

Temperature

The temperature is closely related to the viscosity of a given solution. Accordingly, the consequences of the variation of the solution viscosity would be reflected in the obtained fibers. As well, the temperature increases the rate of evaporation of solvent. The increase in the evaporation of the solvent and the decrease in the viscosity of the solution work by two opposite mechanisms, however, both lead to decrease in the mean fiber diameter [6].

G. Mezzasalma

As a general conclusion of this section, the Tab. 2 summarizes the effect of the different commented parameters on the fiber morphology.

Tab. 2 Electrospinning parameters and their effects on fiber morphology. [30]

	Parameters	Effect on fiber morphology
Solution parameters	Viscosity	Low-beads generation, high increase in fiber diameter, disappearance of beads.
	Polymer concentration	Increase in fiber diameter with increase of molar mass
	Conductivity	Decrease in fiber diameter with increase in conductivity
	Surface tension	No conclusive link with fiber morphology, high surface tension results in instability of the jets
Processing	Applied voltage	Decrease in fiber diameter with increase in voltage
	Distance between tip and collector	Generation of beads with too small and too large distance, minimum distance required for uniform fibers
	Feed rate/Flow rate	Decrease in fiber diameter with decrease in flow rate, generation of beads with too high flow rate
Ambient	Humidity	High humidity result in circular pores on the fibers
	Temperature	Increase in temperature results in decrease in fiber diameter.

3 Materials and methods

3.1 Materials

Polycaprolactone (PCL) was provided by Sigma-Aldrich as 3 mm diameter pellets ($M_n = 80000$ g·mol^{-1}, $T_m = 60$ °C, $\rho = 1.145$ g·mL^{-1} at 25 °C).

Gelatin (Ge) type A, derived from acid-cured porcine skin, was provided by Sigma-Aldrich, with solubility in H_2O at 50 mg·mL^{-1} and gel strength ≈ 300. The density of the Ge was calculated experimentally by making a disk with a hydraulic press. The height and the diameter of the disk were calculated as the average of ten points measured using a micrometer Mitutoyo Comparator Stand 215-611 BS-10M and weighed in a Mettler Toledo XS105 balance. The obtained density of the Ge was $\rho = 0.652$ g·mL^{-1}.

Polyaniline (PAni) emeraldine salt was provided by Sigma-Aldrich as powder with average diameter 3-100 µm ($M_w > 15000$ g·mol^{-1}, conductivity 2-4 S·cm^{-1}, $T_m > 300$ °C, $\rho = 1.360$ g·mL^{-1} at 25 °C). Formic acid was provided by Scharlau ($\geq 98\%$) ($\rho = 1.220$ g·mL^{-1}). Acetic acid was provided by Panreac ($\geq 99\%$) ($\rho = 1.050$ g·mL^{-1}).

3.2 Methods

3.2.1 *Scaffold production*

Solution preparation

The polymer blends of PCL/Ge were prepared by varying the weight percentage of the PCL and Ge to obtain the compositions 40/60, 50/50, 60/40. Moreover, different concentrations of PAni ranging from 0.25% up to 1.00% of the total weight of the blend were added, according to Tab. 3. Solutions for ES were prepared in 1:1 formic/acetic acid, with a polymer concentration of 15 % wt., as suggested in ref. [48], stored in an oven at 30 °C under magnetic stirring and were electrospun after 24, 48, 72 and 96 h of dissolution time.

Tab. 3 Composition of the electrospun scaffolds.

PCL (%wt.)	Ge (%wt.)	PAni (%wt. total)
		-
		0.25
50	50	0.50
		1.00
		-
		0.25
60	40	0.50
		1.00
		-
		0.25
40	60	0.50
		1.00

Electrospinning

Electrospinning was performed by means of a horizontal compact lab-scale setup Bioinicia Fluidnatek® LE-10, which assembled a high voltage source, a programmable syringe pump, a HSW Norm-Ject 20 mL Luer Lock syringe, Teflon® tubing, a gauge 21 metallic needle and a grounded flat collector, as shown in Fig. 10. The tip-to-collector distance was maintained constant at 17 cm. In order to establish a steady state condition and so the formation of the Taylor cone, the voltage and the flow rate varied, as the dissolution time increased, from 1.5 ml to 0.5 ml and between 15-25 kV, respectively. Other factors such as the polymer concentration, needle diameter, tip-to-collector distance, collector type, working time, temperature and humidity remained fixed. Then, the fibers were allowed to evaporate residual solvent at room temperature for 2 h, prior to storing them into zip bags for further analyses.
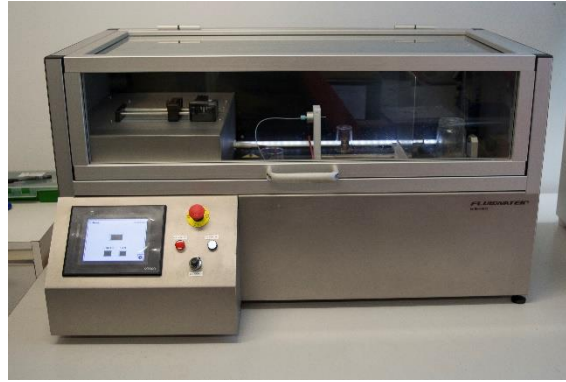
Fig. 10 Electrospinning equipment Bioinicia Fluidnatek LE- 10.

3.2.2 *Scaffold characterization*

Field emission scanning electron microscopy (FE-SEM)

The field emission scanning electron microscope (FE-SEM) is an instrument that offers a wide variety of information about the sample surface with a high resolution. This technique allows to determine the surface morphology, the size of the nanofibers and the cross section of the prepared scaffolds. The operation consists of sweeping the surface of the sample with a beam of electrons, so that the electrons disperse or cause the appearance of secondary electrons that allow visualizing the surface. The FE-SEM uses an electron gun as a source that provides a focused electron beam in a range of voltages (0.02-5 kV). Low voltages improve the spatial resolution and avoid the loading effect in non-conductive samples. The analysis chamber works under vacuum and the electron gun is located in the top part of the chamber.

The microscope model Zeiss Ultra 55 shown in Fig. 11 was used for the operation. To promote the conductivity of the samples a Mitec K950 Sputter Coater was used to create a metallic coating of platinum by sputtering using an electric field in an inert atmosphere, working in vacuum conditions. Once the samples were coated, they were placed onto the sample holders and were introduced into the FE-SEM equipment. The micrographs were taken using a working distance (WD) between 4 to 5 mm and a voltage of 1.00 kV at different degrees of magnification (100×, 1000×, 5000×, 10000×). The diameter of the nanofibers was measured from the average of 100 measurements through the software ImageJ.

Fig. 11 FE-SEM equipment model ZEISS ULTRA 55.

Thermogravimetric analysis (TGA)

The thermogravimetric analysis (TGA) is a technique that allows to evaluate the thermal stability of a sample in different atmospheres. There are dynamic and isothermal tests. In dynamic tests, the sample is subjected to a temperature program with a constant heating rate, recording the changes in the mass of the sample. In isothermal tests, the sample is maintained at the same temperature under isothermal conditions during a certain time interval and the mass variation is recorded. Any change in the mass of the material will denote a physical process (desorption, evaporation) or chemical reaction (decomposition) in the sample and reports the temperature at which it occurs.

The equipment used in this case was a Mettler Toledo thermogravimetric analyzer TGA/STDA 851, as shown in Fig. 12. Samples, with a mass between 3 and 5 mg, were introduced into 70 µl alumina capsules. Next, the samples were placed into the equipment, previously calibrated. The samples were subjected to a dynamic test, based on a heating segment from 25 ℃ to 800 ℃ with a heating rate of 10 ℃·min^{-1}. A test was performed with an empty capsule (blank) to take the reference baseline. The tests were carried out in oxidative atmosphere. For this purpose, an oxygen feed rate of 50 ml·min^{-1} was considered. The samples were studied in triplicate and the averages and deviation were taken as representative values.

Fig. 12 Mettler Toledo TGA / STDA 851 thermogravimetric analyzer.

Differential scanning calorimetry (DSC)

The differential scanning calorimetry (DSC) technique was used to characterize the thermal properties of the scaffolds. This technique is based on a thermo-analytical process that allows to measure the transformation enthalpy, between a sample and a reference as a function dependent on time or temperature. This technique shows and quantifies the different energy transitions that a material can undergo, either by heating or cooling, with or without phase change or by reaction chemistry.

A Mettler Toledo DSC 822e equipment was used, as shown in Fig. 13, coupled with a Haake EK 90/MT cooling system. This technique required the use of an auxiliar balance Mettler Toledo model XS105, 40 μl aluminum capsules previously perforated to allow the release of possible gases released during the test and the small sealing press from Mettler Toledo. Once prepared, the samples were placed into the equipment. One empty capsule was placed to be used as baseline reference. The method of analysis consisted of different consecutive intervals of heating/cooling/heating between 0 ºC and 200 ºC with a speed of 10 ºC·min^{-1}. The test was carried out in an inert nitrogen atmosphere with a flow rate of 50 ml·min^{-1}. The samples were analysed in triplicate and the averages and deviation were taken as representative values.
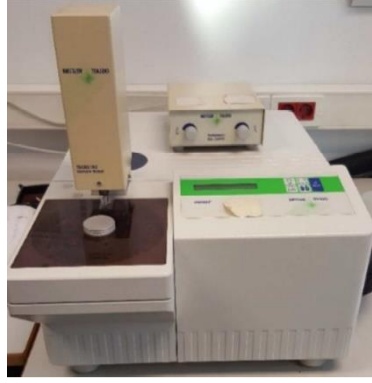
Fig. 13 DSC analyzer Mettler Toledo 822e.

Literature propose that properties such as the fiber morphology, the molar mass, the crystallinity degree or the lamellar thickness play an important influence during the application of a biodegradable biomedical device. Indeed, by adopting a particular fiber morphology (i.e. size scale) and mode of assembly of polymer chains (i.e. crystallinity), it is possible to influence the cell adhesion and proliferation kinetics and further determine the course of their differentiation process [50]. For this purpose, the crystallinity degree and the lamellar thickness were evaluated as below.

Crystallinity degree evaluation

The crystallinity degree (X_c) was evaluated from the melting enthalpy results, by means of the Eq. 1

$$X_c \, (\%) = \frac{\Delta h_m}{w_{PCL} \cdot \Delta h_m^0} \cdot 100 \qquad \text{Eq. 1}$$

where Δh_m is the melting enthalpy of the PCL, w_{PCL} is the weight fraction of the PCL in the sample and Δh_m^0 is the melting enthalpy of a perfect crystal of PCL (148 J·g^{-1}) [51].

Lamellar thickness evaluation

In order to deeply characterize the crystalline structure of the scaffolds, the lamellar thickness (l_c) were calculated by applying the Thomson-Gibbs equation (Eq. 2), based on the temperatures associated to peak of the melting transitions [52]–[55].

$$l_c(T_m) = \left[\left(1 - \frac{T_m}{T_m^0} \right) * \frac{\Delta h_{mv}}{2 \cdot \sigma_e} \right]^{-1} \qquad \text{Eq. 2}$$

where T_m is the melting temperature; T_m^0 is the equilibrium melting temperature of an infinite crystal (348 K), σ_e is the surface free energy of the basal plane where the chains

28

fold ($106 \cdot 10^{-3}$ J·m^{-2}) and Δh_{mv} is the melting enthalpy per volume unit ($1.63 \cdot 10^{8}$ J·m^{-3}) [56].

Fourier transform infrared spectrometry (FT-IR)

The Fourier Transform Infrared Spectrometry (FT-IR) is a technique used to determine the molecular structure of a given substance based on the interaction between an infrared radiation and the irradiated sample. As the radiation is absorbed by the sample, net changes of charge occur in the rotational and vibrational levels of the molecules, which is reflected in the infrared spectra as several absorption bands. Vibrations can cause changes in the length of the bond (extension) or angle (bending) as they may occur symmetrically or asymmetrically. The equipment collects the resulting signal (interferogram) and provides information on the amount of energy absorbed by the sample. The interferogram must be converted to the domain of frequencies to provide information on the identification of substances, identification and quantitative determination of final groups and determination of ramifications.

The equipment used was a Thermo Nicolet ™ 5700 FT-IR spectrometer, shown Fig. 14. In this case, the equipment was coupled with a specific module for measuring solid samples, through the measurement of total attenuated reflectance (ATR). The IR spectrum was taken between the wavelengths of 4000 cm^{-1} and 400 cm^{-1} with a resolution of 4 cm^{-1} over 64 sweeps. Initially, a trial was carried out without sample with the aim of establishing the baseline of the subsequent trials. Then, up to 5 trials were made from different points of the same sample and the average spectra were taken as representative.

Fig. 14 Thermo Nicolet^{TM} 5700 FT-IR spectrometer.

G. Mezzasalma

Size exclusion chromatography (SEC)

Size-exclusion chromatography (SEC) is a chromatographic method in which molecules in solution are separated by their size, which can be correlated to the molar mass of the polymer. Typically, an eluent solution is used to transport the sample through the column, which is packed with fine, porous beads. The pore sizes of these beads are used to estimate the dimensions of macromolecules. SEC is a widely used polymer characterization method because of its ability to provide valuable results from the molar mass distribution for polymers.

The SEC analyses were carried out by means of a Malvern Instruments Omnisec Resolve chromatograph. (Fig. 15). It combines an integrated pump, a degasser, an autosampler and a column oven, along with a Malvern Instruments Omnisec Reveal multi-detector, Ultraviolet (UV), Refractive Index (RI), Low and Right Angle Light Scattering (LALS and RALS) and Viscosity (VISC). A monodisperse polystyrene standard with dn/dc value of 0.185 was used for previous calibration. Two columns from Malvern Instruments (T2000 and T4000) were used (300×8 mm). Tetrahydrofuran (THF) was used as mobile phase at a flow rate of 1 mL·min^{-1} and a column temperature of 35 ºC. The samples were dissolved in THF with concentrations of around 2.0 mg·ml^{-1} and filtered through 0.45 µm PTFE filters. Two replicates per sample were performed and the obtained data were analyzed with the aid of the Omnisec V10™ software.

Fig. 15 Malvern instruments Omnisec Resolve chromatograph.

Hydrolytic degradation model

In order to predict the decrease of the molar mass as a function of the initial solution concentrations and time, analytical equations adopted by Lavielle et al. [47], were used.

30

The model used by Lavielle et al. describes the degradation of polyesters developed by Pitt and Gu [57] and Lyu et al. [58]. Pitt and co-workers proposed that normal hydrolysis follows first order kinetics in absence of catalytic effects, whereas autocatalytic hydrolysis follows second order kinetics. In the derivation of this model it is assumed that the degradation follows pseudo-first order kinetics. Only the carboxylic acid concentration is taken into account, whereas the concentration of ester bonds is ignored, while the reaction rate of hydrolysis depends on both concentrations. In the work of Lyu et al. the authors assumed that the rate of degradation depends on both the concentration of breaking bonds and water. For that a second order kinetic equation is derived. However, the autocatalytic effect of the formation of degradation products is neglected and it is also assumed that the water concentration within the polymer stays constant. The obtained rate equation is a first order rate equation, which is used as a basis for a model describing both the bulk degradation of a polymer and the mass loss during surface degradation or degradation with a moving erosion front in the polymer. Lavielle et al. assumed the absence of autocatalysis as the acid concentration is much larger than the ester and water concentrations.

The use of this approach was suitable for our system, considering the PCL in a mixture of acetic and formic acid (50/50, v/v) with a concentration of 15% (w/v)), as PCL was fully solubilized in the acid mixture and thus all ester bonds had the same probability of reacting with water at a given time [59]. For the model, variable water and ester concentrations and a constant acid concentration was imposed, which was a realistic hypothesis, because the acid amount largely exceeded the water quantity [60].

Due to the low amount of water in the acidic solutions (1.1 %wt., stated by the manufacturer), the equilibrium was considered to be shifted towards the hydrolysis direction and neglected secondary reactions such as transesterification [60]. Thank to these considerations, it is possible to describe the evolution of the newly yielded alcohol concentration, u, through a second order equation (Eq. 3) and from it express theoretical number average molecular weight (M_n) as a function of time (Eq. 4):

$$\frac{du}{dt} = kEW \ [mol \cdot L^{-1} \cdot s^{-1}] \qquad \text{Eq. 3}$$

$$M_n(t) = \rho \frac{E_0 e^{k(E_0 - W_0)t} - W_0}{(W_0 + u_0)E_0 e^{k(E_0 - W_0)t} - W_0(E_0 + u_0)} \ [g \cdot mol^{-1}] \qquad \text{Eq. 4}$$

in which u_0 is the initial concentration of alcohol groups (mol·L^{-1}); k is the second-order hydrolysis rate constant (L·mol^{-1}·s^{-1}); E_0 is the initial concentration of ester bonds (mol·L^{-1}); W_0 is the initial concentration of water molecules (mol·L^{-1}); and ρ is the weight concentration of polymer (g·L^{-1}).

Dielectric-thermal impedance spectrometry (DETS)

The dielectric-thermal impedance spectrometry (DETS) technique is based on the use of an alternating current (AC) signal that is applied to an electrode and on the measure of the response caused. Generally, experiments are carried out by applying a small potential (*E*) to an electrode and measuring the response in the current values (*I*) at different frequencies. In this way, measurements of potential, time and current are obtained giving, as a result, measurements of impedances and frequencies in the so-called spectrum of impedances. The impedance (*Z*) is a term that describes the electrical resistance used in alternating current (AC) circuits. In the case of a direct current circuit (DC), the resistance is defined as a relationship between the potential (*E*) and the current (*I*) by Ohm's law [61].

$$R(\Omega) = \frac{E(V)}{I(A)} \qquad \text{Eq. 5}$$

In the case of alternating current (AC), it is defined as:

$$E(V) = I \cdot Z \qquad \text{Eq. 6}$$

where *Z* represents the impedance of the circuit in ohms (Ω), each value of *Z* depends on the frequency of the applied signal (*f*), which measured in Hertz (*Hz*).

In the AC circuit, there are other elements that compose the circuit, apart from the resistance (*R*), as the capacities (*C*) or inductances (*L*). These elements impede the flow of electrons through the electrical circuit. The inductance (*L*) is the voltage induced by the magnetic field in the conductor while the capacity (*C*) is the electrostatic charge storage induced by the voltage between the conductors. The combination of both elements is called reactance (*X*) [61].

The impedance of a system at each frequency is defined as the ratio between the amplitude of the alternating current signal and the amplitude of the alternate potential signal and the

phase angle. The mathematical development of this theory defines the impedance of a system in terms of a real component and an imaginary component following the equation:

$$|Z|(\Omega) = \sqrt{Z_r + Z_j} \qquad \text{Eq. 7}$$

Where the real part corresponds to the quantized value of the impedance (*Z*) of a circuit and the imaginary part with the reactance (*X*). The phase angle is related to the impedance by the following expression:

$$\theta = tan^{-1}\left(\frac{Z_j}{Z_r}\right) \qquad \text{Eq. 8}$$

The spectrometry equipment performs precise measurements of the complex dielectric function, conductivity and impedance in materials in the frequency and temperature domain. The analysis is carried out by measuring the impedance *Z(f)* of a capacitor formed by two or more electrodes with the sample material in between at a controlled temperature. From *Z(f)*, the complex spectra *ε(f)* and conductivity *σ(f)* are evaluated. This technique allows the analysis of the molecular dynamics of polymer systems in a frequency range from 10^{-2} to 10^9 Hz temperature from -150 ºC to 300 ºC. The key parameters obtained by the equipment are the frequency range, impedance range and the phase angle.

The impedance measurements were made using the equipment Novocontrol Broadband Dielectric Impedance Spectrometer (BDIS) connected with a Novocontrol Alpha-A Frequency Response Analyzer, shown in Fig. 16. A BDS-1200 Novocontrol parallel-plated capacitor with two plated electrodes system was used as dielectric cell test. The scaffold thickness was evaluated using a micrometer Mitutoyo Comparator Stand 215-611 BS-10M taking the average of 6 measurements in different positions of the sample. Next, it performed a single sweep at room temperature (25 ± 1 °C) in a frequency range from 10^{-2} to 10^7 Hz. The electric conductivity (σ_{elec}) was considered at low frequencies, where the measured real part of the conductivity (σ') reaches a plateau that is correlated to the DC conductivity ($\sigma 0$).

Fig. 16 Novocontrol Broadband Dielectric Impedance Spectrometer (BDIS).

3.2.3 *Nanofibers validation*

Hydrolytic degradation in physiologic conditions

The PCL/Ge based scaffolds were subjected to hydrolytic degradation in phosphate buffer solution (PBS), according to international norm ISO 10993-13:2010, method 4.3 [62]. The initial electrospun scaffolds were cut into rectangular specimens with a mass around 10 mg. The specimens were weighed (m_0) and placed in a previously weighed vial (m_{vial}). 10 mL of degradation medium were introduced and then the vials were sealed with polytetrafluoroethylene (PTFE) threaded plugs and placed in a thermostatically controlled oven at 37 ºC. The pH of the PBS solution was adjusted to 7.4 with NaOH 1 M. The effects of the hydrolytic degradation were evaluated after 100 days of immersion. Then, the scaffolds followed a washing-drying-keeping procedure. Accordingly, samples were dried under vacuum to constant mass into their degradation vials (m_{dry}) and saved for further analyses. The mass loss of the specimens was calculated according to Eq. 9.

$$Mass \; \% = \frac{m_{dry} - m_{vial}}{m_0} \cdot 100 \qquad \text{Eq. 9}$$

4 Results and discussion

In this section, the developed scaffolds were assessed in terms of:

- validation of the biocompatibilization strategy (PCL/Ge) by analyzing the scaffold obtained after 24 h of dissolution time to ensure the presence of Ge in the scaffolds.
- corroboration of the functionalization strategy (PCL/Ge/PAni), by studying the samples obtained after 24 h of dissolution time to confirm the presence of PAni in the scaffolds.
- evaluation of the effect of the dissolution time on their main physico-chemical properties by testing all the scaffolds obtained at all the dissolution times.

4.1 Biocompatibilization strategy: PCL/Ge blending

In order to verify the biocompatibilization by means of the certification of existence of gelatin in the blended scaffolds, the scaffold morphology, the chemical structure, the thermo-oxidative stability and the thermal properties were assessed. For this purpose, field-emission scanning electron microscopy, Fourier transformed infrared spectroscopy, thermogravimetric analysis and differential scanning calorimetry were considered. The use of these techniques allows to understand if the Ge was correctly electrospun in the nanofibrous scaffold with the established concentrations. In this section, scaffolds with different PCL/Ge ratios after a dissolution time of 24 h were selected.

4.1.1 *Microscopic appearance*

The surface electronic micrographs of the developed scaffolds, as obtained by field emission scanning electron microscopy (FE-SEM) are gathered in Tab. 4. As perceived from the electronic micrographs, the fiber diameter remained in the nanoscale range for all the studied compositions. In general, uniform, non-woven nanofibers were observed in all cases.

Tab. 4 Surface electronic micrographs of PCL/Ge based scaffold.

PCL/Ge		
60/40	**50/50**	**40/60**
110±44 nm	183±38 nm	185±50 nm
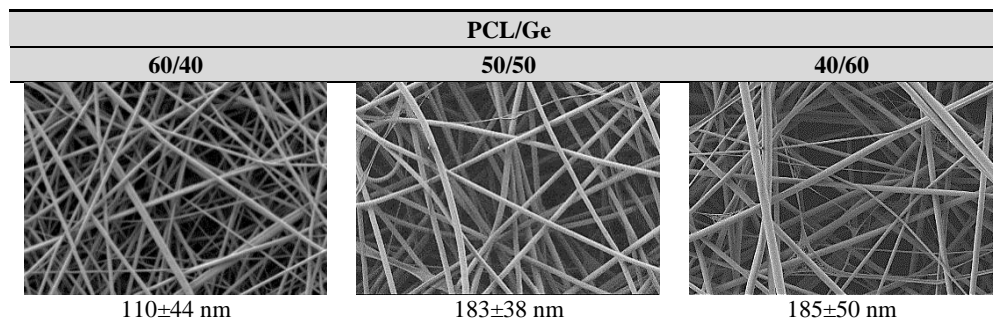
Fig. 17 shows the histogram plots of the fiber diameter distribution and the average fiber diameter of the electrospun scaffold as a function of the PCL/Ge concentration ranging from 60/40 to 40/60, as measured from the micrographs in Tab. 4.

The increase of the Ge content in the materials resulted in an increase of the average fiber diameter from mean values of 116 nm for the 60/40 concentration to 185 nm for the 40/60 concentration.
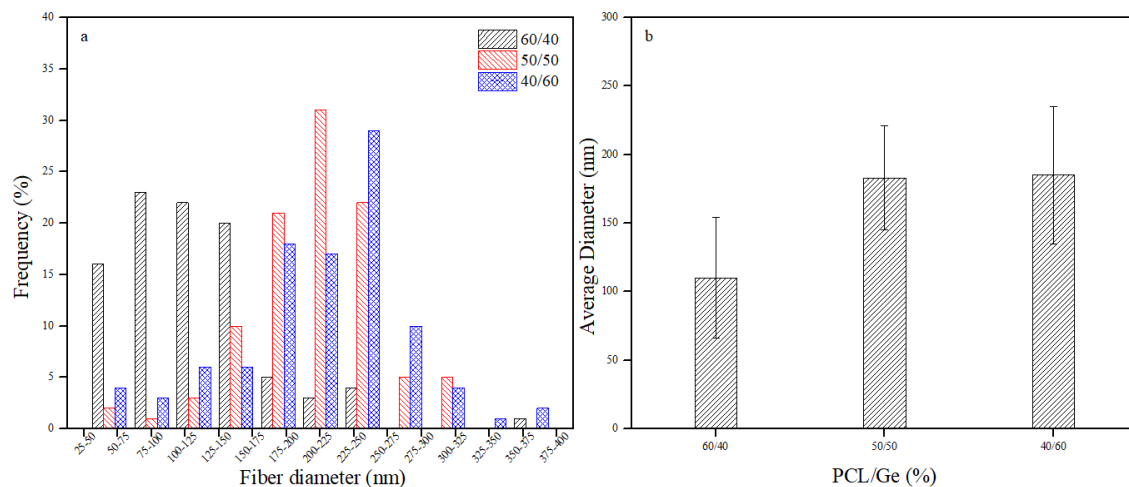
Fig. 17 Fiber diameter distribution (a) and average fiber diameter with the band error (b) (mediated over 100 measurements) as a function of PCL/Ge %.

4.1.2 *Chemical composition*

The Fig. 18 shows the pure PCL and Ge infrared spectra along with that of the electrospun scaffolds. As observed, the characteristic peaks of pure PCL, Ge and PCL/gelatin scaffolds were found, which were correlated to the bands at 1727 cm^{-1} of the C$=$O stretching vibration in carbonyl groups, 2865 cm^{-1} of the symmetric CH$_2$ stretching, and

2950 cm^{-1} of the asymmetric CH$_2$ stretching. The characteristic peaks of gelatin appeared at approximately 1650 cm^{-1} (amide I), 1540 cm^{-1} (amide II), and 3300 cm^{-1} (amide A), which were related to the stretching vibrations of C═O bonds, the coupling of the bending of N─H and the stretching of C─N bonds, and the N─H stretching vibration, respectively [7].
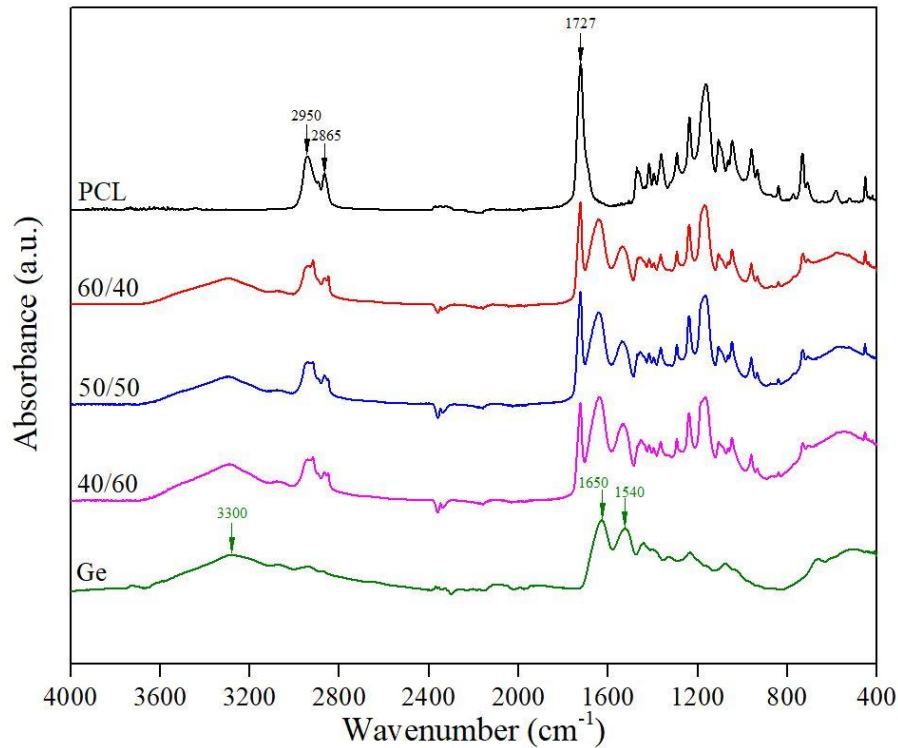
Fig. 18 FTIR spectrum and intensities of pure PCL and Ge and three different PCL/Ge blends.

4.1.3 *Thermo-oxidative stability*

Thermo-oxidative stability of PCL, Ge and PCL/Ge blended scaffolds were performed using the thermogravimetric analysis (TGA) technique. From Fig. 19 appears that PCL showed two thermal degradation stages, while the Ge degraded in three stages. PCL decomposed almost completely in the region of 300 °C to 450 °C, as confirmed by Gautam et al.in their study on the thermal degradation of PCL, Ge and their blends, with a peak temperature (T$_p$) of 394.7 °C, as shown in the derivative curve of weight loss (DTG) in Fig. 19 and indicated in Tab. 5. The first stage of gelatin weight loss (Δm), from 50 °C to 150 °C (T$_p$ 88.91 °C) can be described as moisture vaporization [63], [64], while the second stage starting around 250 °C and completing around 450 °C, is the main thermal degradation zone and it corresponds to a complex process including protein chain

breakage and peptide bond rupture [63]. PCL/Ge composite scaffolds showed a four-step thermal degradation, as indicated in the DTG chart (Fig. 19).

The step 1 corresponds to the gelatin (50-150 °C), showing an increasing Δm and T range with the increase of the Ge concentration, the same behavior appeared for the step 2 during which there is an increase on the T_p from 312.52 °C of the pure gelatin to 330.62 °C of the 60/40 blended scaffold, as shown in Tab. 5. Here, in PCL/gelatin composite scaffold, lower T_p of gelatin has shifted towards higher T_p of PCL that indicates some interactions between PCL and gelatin in the composite scaffold, as stated in [63]. Step 3 corresponds to the PCL degradation, showing an increase in Δm when its concentration grows, with peaks ranging around 394 °C. Last step (around 450 °C), that is in common with all the 5 samples, corresponds to the final residues' degradation.
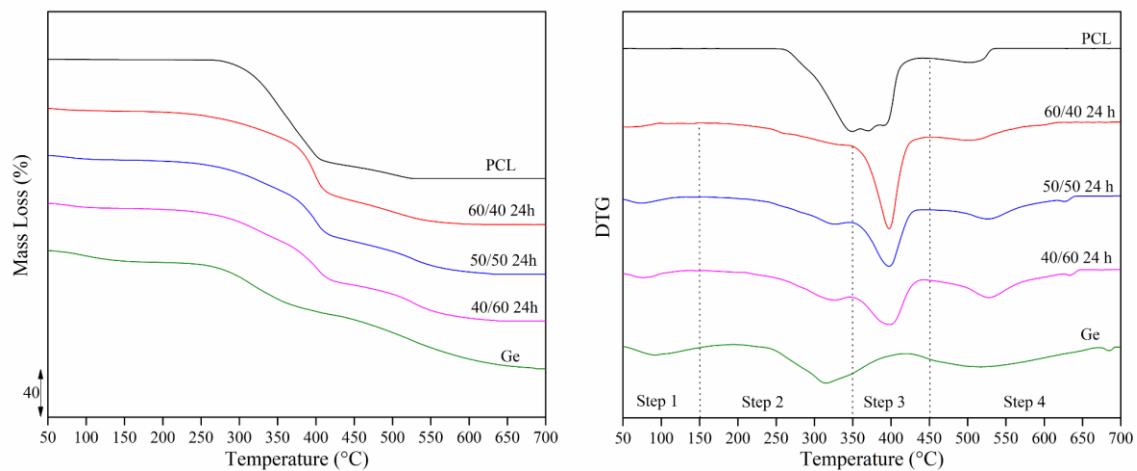
Fig. 19 Mass loss and DTG curves of PCL/Ge at different concentrations

Tab. 5 T peak and weight loss % in function of the PCL/Ge concentration

PCL/Ge	Step 1		Step 2		Step 3		Step 4	
(%)	T_p	Δm (%)	T_p	Δm (%)	T_p	Δm (%)	T_p	Δm (%)
pellet	-	-	-	-	394.07	83.94	503.25	12.93
60/40	55.96	3.74	330.62	30.55	393.61	38.45	503.09	24.13
50/50	74.73	4.70	323.57	33.67	393.91	28.82	527.23	31.18
40/60	73.65	5.16	323.03	35.42	394.67	24.09	528.32	33.18
0/100	88.91	9.83	312.52	37.70	-	-	517.38	43.08

4.1.4 *Thermal properties*

The thermal properties were assessed by means of differential scanning calorimetry (DSC). Fig. 20 shows the endothermal peaks of pure PCL and Ge and the blended scaffolds at a heating/cooling rate of 10 °C/min from 0 °C to 200 °C, while Tab. 6 summarizes the thermal parameters obtained during the heating/cooling processes.

As obtained from Fig. 20 and Tab. 6, PCL had a melting peak (T_m) around 61-62 °C as well as the 60/40 scaffold, while the melting peak of the 50/50 and 40/60 scaffolds decreased to 59-60 °C as the gelatin content increased. In the same way a decrease of the melting enthalpies (ΔH_m) with a minimum for the 40/60 configuration. Meanwhile, pure PCL showed a crystallization peak (T_c) at 20.51 °C, while the blended configurations 60/40, 50/50 and 40/60 (PCL/Ge) exhibit peaks at 26.78 °C, 28.22 °C and 26.91 °C, respectively. During the heating process the Ge, from 70 to 120 °C, underwent water evaporation shown by the hump in the heating chart [63]. These data indicated that gelatin was successfully electrospun into fibrous scaffolds.

Tab. 6 Melting and crystallization temperatures and enthalpies of different PCL/Ge concentrations

PCL/Ge	ΔH_m	T_m	ΔH_c	T_c
%	(J/g)	(°C)	(J/g)	(°C)
pellet	68.43	61.62	-50.72	20.51
60/40	39.4	62.02	-35.75	26.78
50/50	38.94	59.91	-26.17	28.22
40/60	19.84	59.88	-15.86	26.91
0/100	-	-	-	-
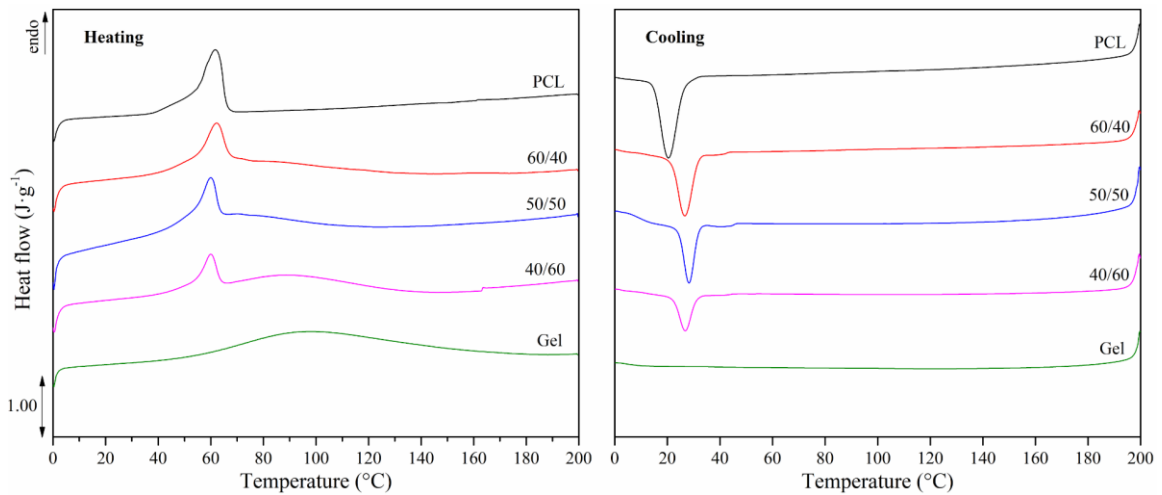
Fig. 20 DSC of pure PCL and Ge and PCL/Ge scaffolds with different concentrations.

4.1.4.1 Crystallinity degree of the PCL fraction

Fig. 21 shows the X_c of pure PCL pellet and PCL/Ge electrospun scaffolds at different concentrations, evaluated by using the Eq. 1. As plotted in the chart the crystallinity degree of the pure PCL pellet was calculated on the range of 45.5-46.5%, reaching a maximum for the 60/40 configuration at $\approx 48\%$. Regarding the remaining scaffold the X_c decreased rapidly, ranging from a minimum at 26.61% of the 50/50 configuration up to 33.51 % of the 40/60 configuration.
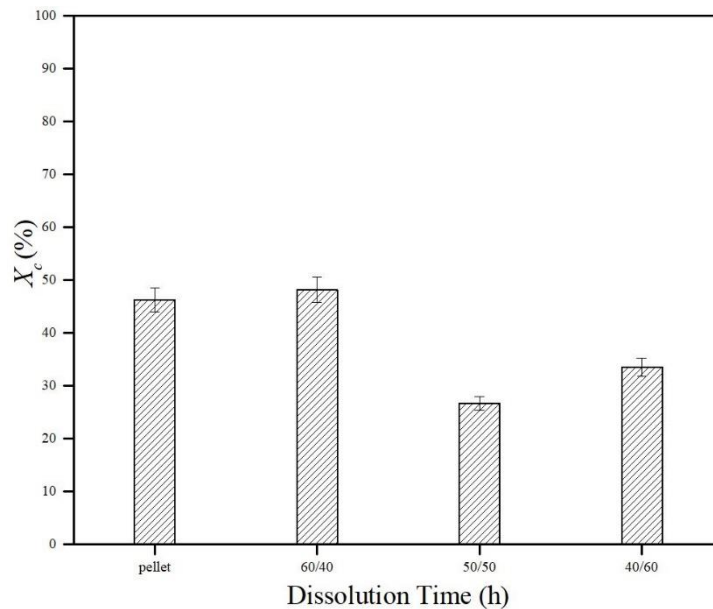
Fig. 21 Crystallinity degree of pure PCL pellet and PCL/Ge scaffolds at different concentrations.

4.2 Functionalization strategy: PAni incorporation

With the aim to corroborate the existence of PAni in the scaffold spectroscopic analyses by means of Fourier transformed infrared analyses (FTIR) and the measurement of the electric conductivity were carried out. To do that 60/40, 50/50 and 40/60 scaffolds including PAni in the different concentrations after 24 h of dissolution time were analyzed using the above-mentioned techniques.

4.2.1 *Microscopic appearance*

The surface electronic micrographs of the developed scaffolds, as obtained by field emission scanning electron microscopy (FE-SEM) are gathered in Tab. 7.

As shown in Fig. 22 the addition of PAni is not so evident even at the highest concentration (1% wt.). For this reason, the FTIR spectra analysis and an electrical conductivity analysis must be done to confirm the suitable functionalization of the scaffolds with the PAni particles in the nanofibers.

Tab. 7 surface electronic micrographs of PCL/Ge/PAni at different concentrations scaffold.

	PAni % wt.			
	0.00	0.25	0.50	1.00
60/40	110±44 nm	116±45 nm	116±53 nm	114±48 nm
50/50	183±38 nm	165±53 nm	161±47 nm	174±63 nm
40/60	185±50 nm	209±56 nm	225±57 nm	181±53 nm

(PCL/Ge % wt. labels the rows.)
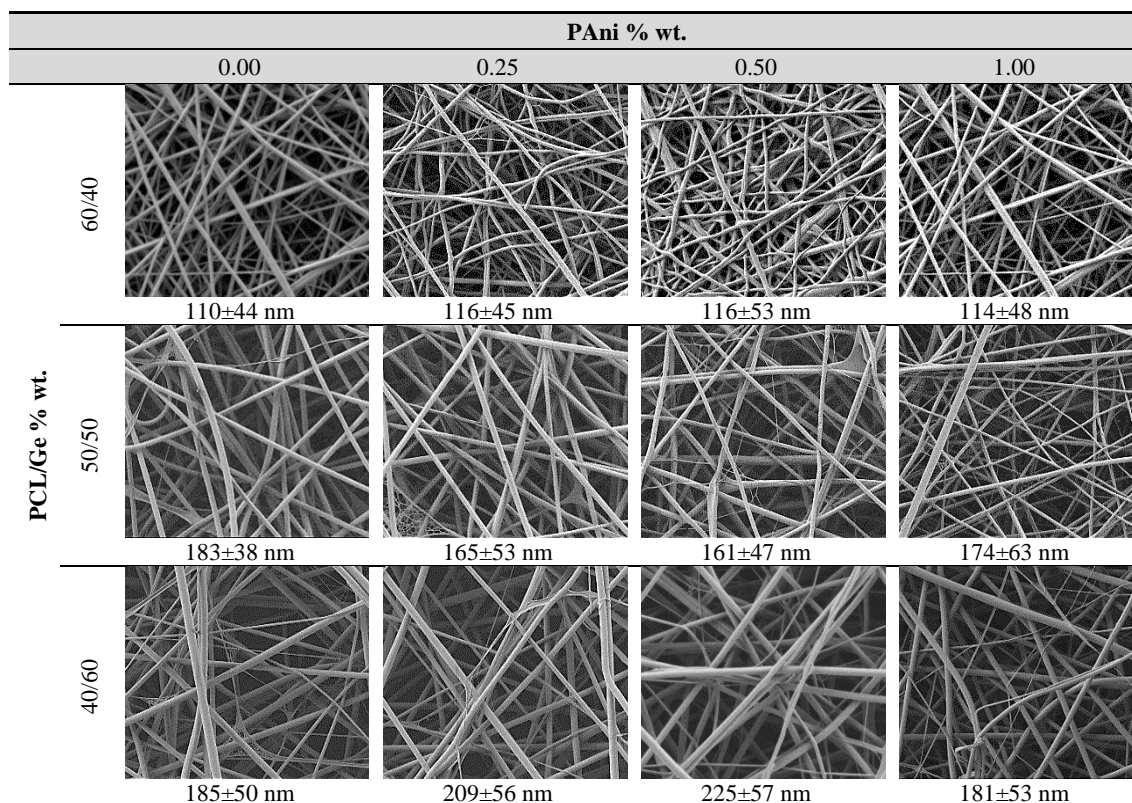
4.2.2 *Chemical composition*

The Fig. 22 shows the FTIR spectra of PCL/Ge nanofiber-scaffold containing PAni at different concentrations, starting from 0.25% wt. to 1.00% wt.

The spectra of PAni usually shows the main bands in the region of 1590, 1508 and 1308 cm^{-1}, corresponding to the ring-stretching vibrations of the quinoid and benzenoid rings of aniline and nitro aniline, respectively [40]. However, these peaks are not present in the obtained spectra, maybe due to the too low concentration of PAni, while are evident all the peaks typical of PCL and Ge commented in the previous section. As well, the absence of the PAni characteristic peaks could be correlated to a good dispersion into the scaffolds. This result suggested that an electric conductivity analysis should be performed to ensure the presence of PAni in the scaffolds.
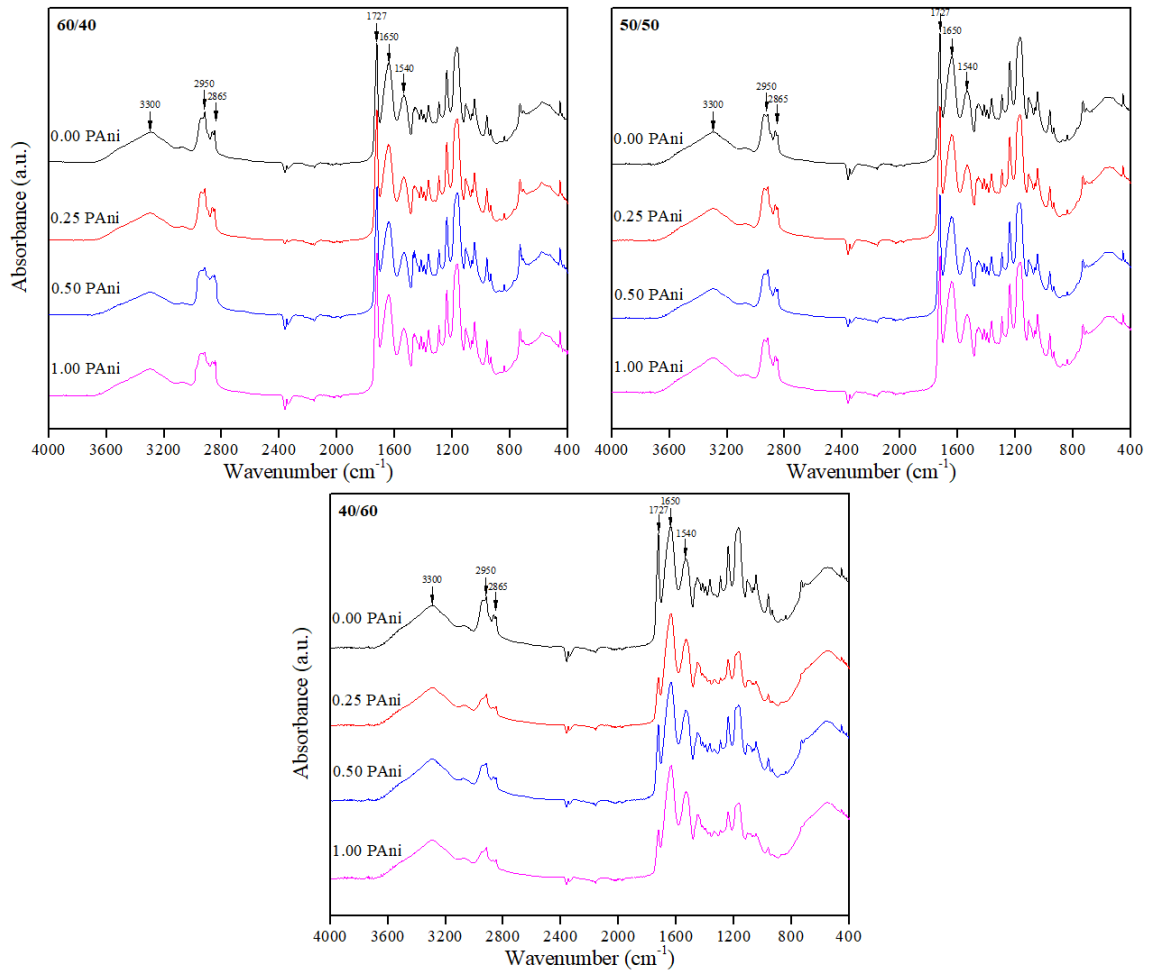
Fig. 212 FTIR spectrum and intensities of PCL/Ge/PAni blended scaffold at different concentrations.

4.2.3 *Electric conductivity*

The conductivity of the nanofibrous scaffolds was assessed by means of dielectric-thermal impedance spectrometry (DETS).

As shown in Fig. 23, the addition of PAni resulted in a quite linear grow in conductivity for the PCL/Ge/PAni scaffolds, with an apparent increase with the Ge concentration, showing a maximum for the 50/50 configuration [41]. This increase in the electrical conductivity corroborated the functionalization of scaffolds through the addition of PAni and certified that it was correctly incorporated in the nanofibrous scaffolds [35].
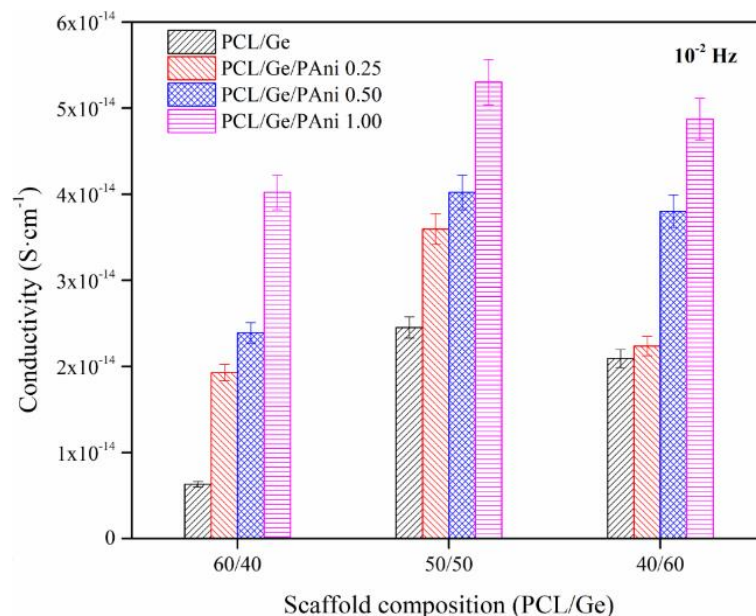
Fig. 22 Electrical conductivity at 10⁻² Hz of PCL/Ge/PAni nanofibrous scaffolds at different concentrations

Recent studies used electrical conducting fiber-scaffolds, showed enhanced outgrowth under electrical stimulations [41]. Accordingly, the electrically conducting PCL/Ge/PAni nanofibrous scaffolds may be considered for electrical-stimulated cell growth applications. Even if the PAni showed a positive effect on the conductivity increase, this is still too low compared with other researches, in which the conductivity is in the order of 10^{-4} S·cm^{-1} [65], [66]. In this way an increase in the PAni concentration could be suggested to achieve a useful conductivity of the scaffolds.

4.3 Tailoring strategy: Dissolution time

In order to investigate the effects of hydrolytic degradation due to the acidic solvent mixture of 1:1 formic/acetic acid during different dissolution time, the nanofiber appearance, thermo-oxidative stability, thermal properties and molar mass were assessed by means of thermogravimetric analysis (TGA), differential scanning calorimetry (DSC) and size exclusion chromatography (SEC). All these techniques may allow to corroborate the chain scission is influenced by the dissolution time of the polymer blends in the acidic solvent mixture.

4.3.1 *Microscopic appearance*

The dissolution time had a substantial influence on the fiber diameter. In fact, as shown in Tab. 8, Tab. 9 and Tab. 10, a significant decreasing tendency with higher dissolution time was observed. Bead-free fibers were found for shorter dissolution times, 24 h and 48 h respectively, while some beads appeared for higher dissolution times, 72 h and 96 h respectively. In particular, it seems that beads appearance decreased with increasing of Ge content.

Fig. 24 shows the histogram plots of the average fiber diameter of the electrospun scaffold after 24, 48, 72 and 96 h of dissolution time in the hydrolytic acid solvent, as measured from the micrographs.

The variation in the PCL/Ge content showed a decrease in the fiber diameter from mean values of 116 nm to 37 nm for 24 h and 96 h, with the 60/40 concentration scaffold; from 183 nm to 44 nm for 24 h and 96 h for the 50/50 concentration; and from 225 nm to 77 nm for 24 h and 96 h, in the case of 40/60 concentration.

As shown in Fig. 25, which plot the histograms of fiber diameter distribution, there is a clear decrease in the fiber diameter dimension going from 24 h to 96 h of dissolution time. The reduction of the fiber diameter for a given composition during electrospinning is usually correlated to a lower solution viscosity, caused by the hydrolytic action of the solvent and the subsequent lower incidence of chain entanglements [47], [50], [67]. In this context, the changes in the polymer, especially in the PCL fraction, when diluted in

the acidic mixture may have been the cause of the lower solution viscosity, correlated to less entanglement capability, with subsequent reduction of the fiber diameter.
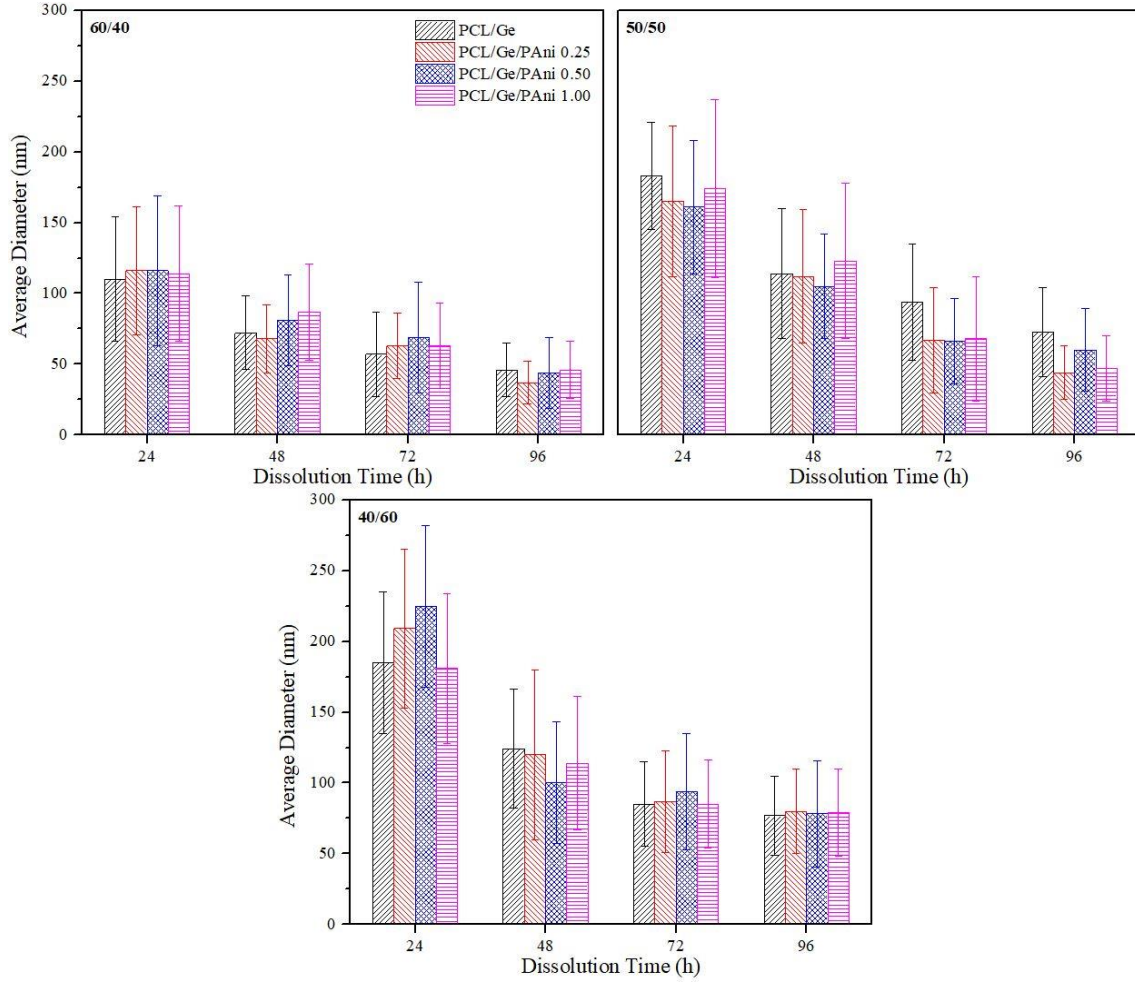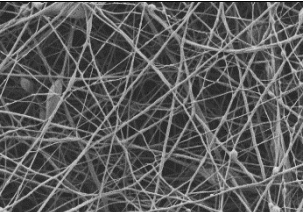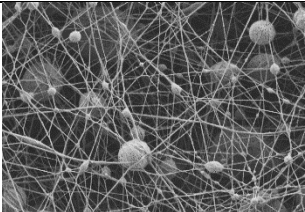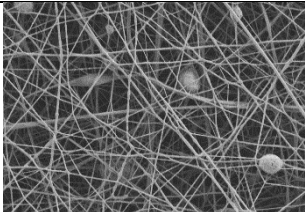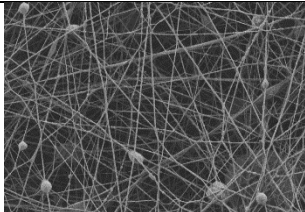

Fig. 23 Average fiber diameter with the band error (mediated over 100 measurements) as a function of the dissolution time.

Tab. 8 surface electronic micrographs of 60/40 PCL/Ge based scaffold.

PCL/Ge % wt.	60/40			
PAni % wt.	0.00	0.25	0.50	1.00
Dissolution Time (h) 24	110±44 nm	116±45 nm	116±53 nm	114±48 nm
48	72±26 nm	68±24 nm	81±32 nm	87±34 nm
72	57±30 nm	63±23 nm	69±39 nm	63±30 nm
96	46±19 nm	37±15 nm	44±25 nm	46±20 nm
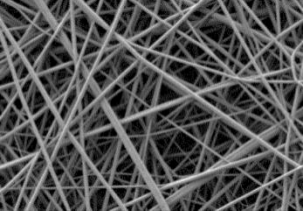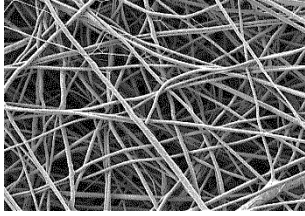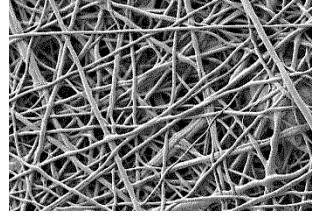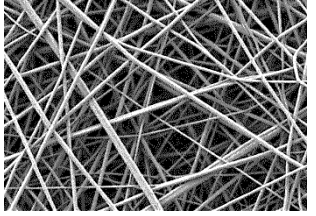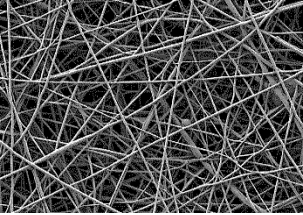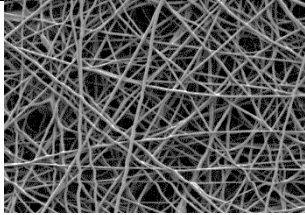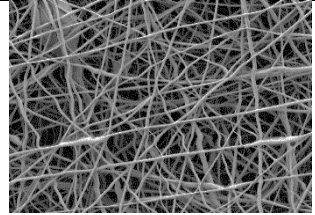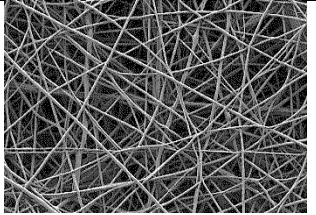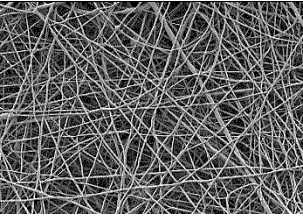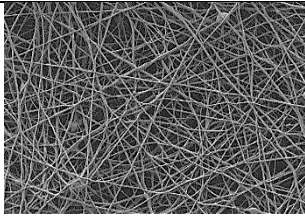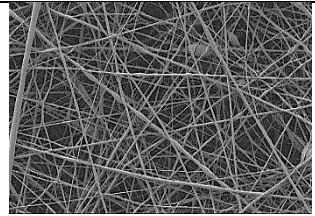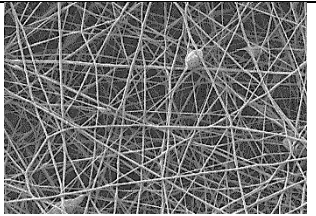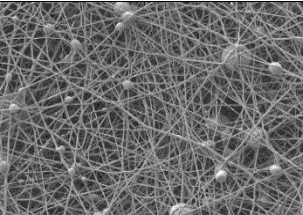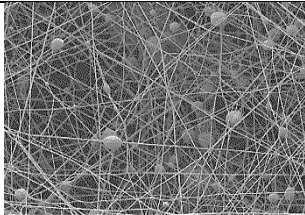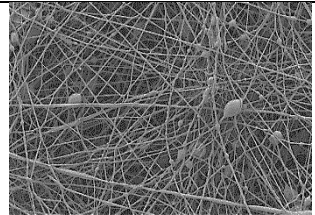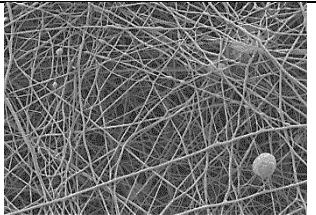
Tab. 9 surface electronic micrographs of 50/50 PCL/Ge based scaffold
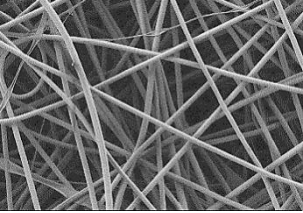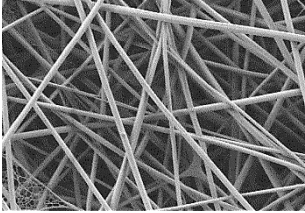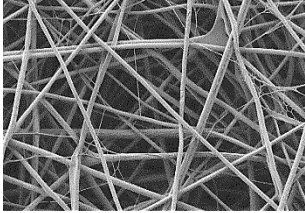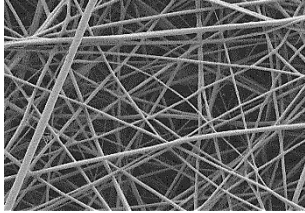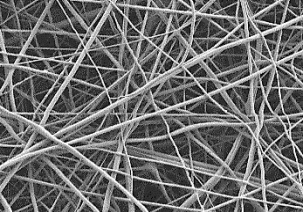
PCL/Ge % wt.	50/50			
PAni % wt.	0.00	0.25	0.50	1.00
24	183±38 nm	165±53 nm	161±47 nm	174±63 nm
48	114±46 nm	112±47 nm	105±37 nm	123±55 nm
72	94±41 nm	67±37 nm	66±30 nm	68±44 nm
96	73±31 nm	44±19 nm	60±29 nm	47±23 nm
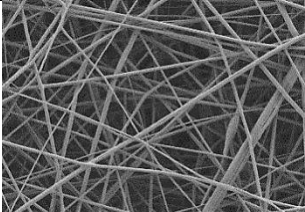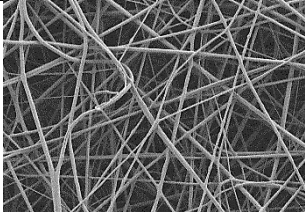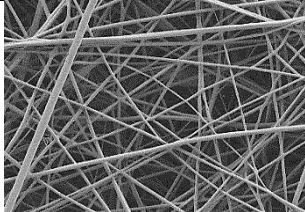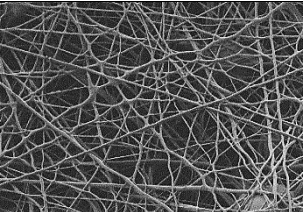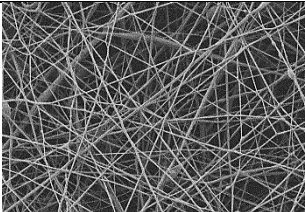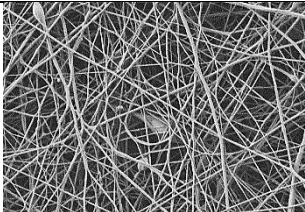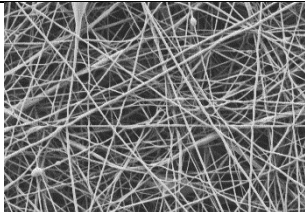
Dissolution Time (h)

Tab. 10 surface electronic micrographs of 40/60 PCL/Ge based scaffold

PCL/Ge % wt.	40/60			
PAni % wt.	0.00	0.25	0.50	1.00
24	185±50 nm	209±56 nm	225±57 nm	181±53 nm
48	124±42 nm	120±60 nm	100±43 nm	114±47 nm
72	85±30 nm	87±36 nm	94±41 nm	85±31 nm
96	77±28 nm	80±30 nm	78±38 nm	79±31 nm
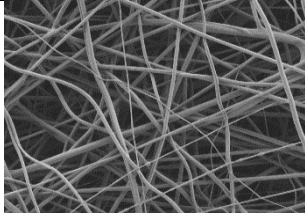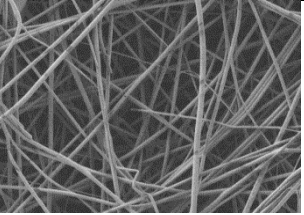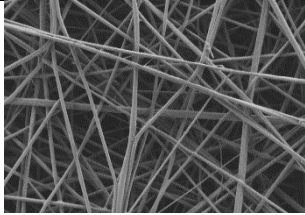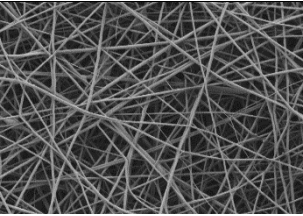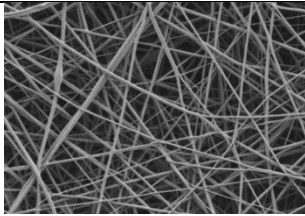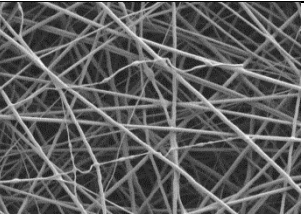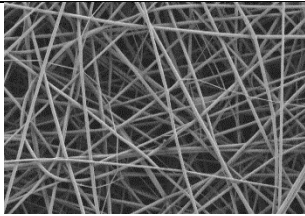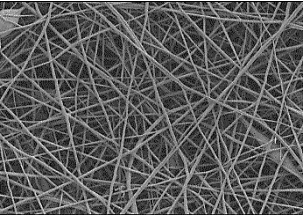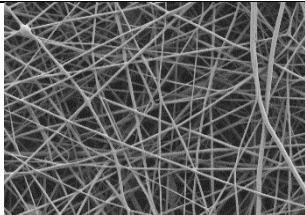
Dissolution Time (h)
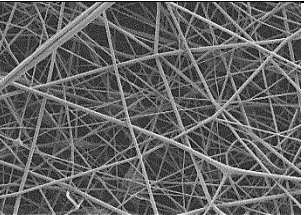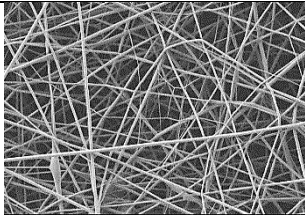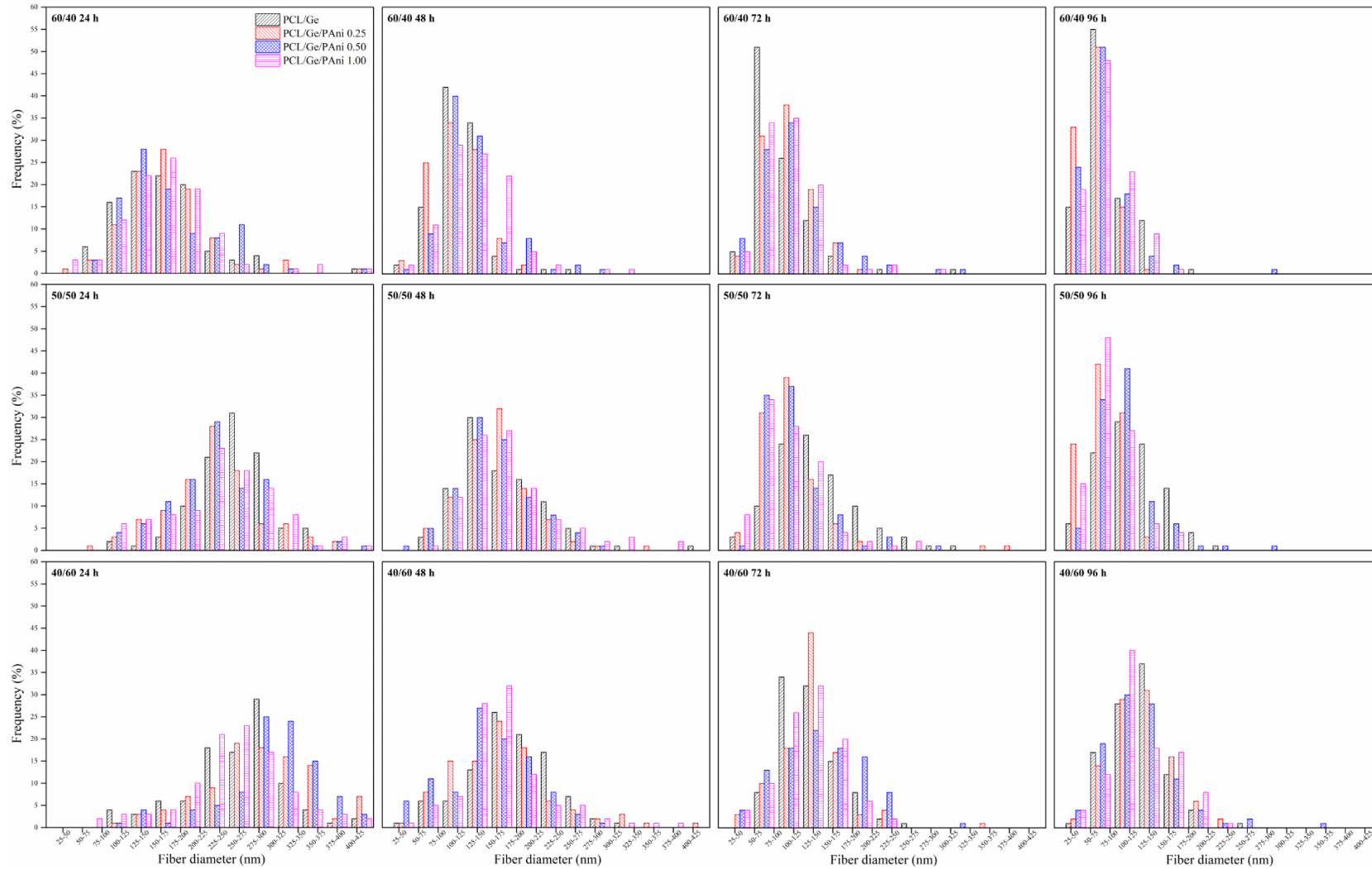
Fig. 24 Fiber diameter distribution.

4.3.2 *Thermo-oxidative stability*

The evaluation of the thermo-oxidative stability may bring valuable information about the state of the polymers that constitute the blends. In this line, thermogravimetric analyses (TGA) were carried out. Fig. 26 and Fig. 27 show respectively the TG and DTG curves of the blended scaffolds at different concentrations and different dissolution times, while Tab. 11 shows the peak temperatures of the weight loss processes.

As seen before, all the composite scaffolds showed a four steps thermal degradation, as reported in the DTG chart in Fig. 27. The first two steps corresponded to the Ge degradation, corresponding to the moisture vaporization and Ge denaturation [63] [64]. The third step corresponded to the PCL degradation; this stage showed a general shift of the T_p to lower values going from a 24 h of dissolution time to a 96 h of dissolution time, with all the values of T_p reported in Tab. 11. This behavior suggested that the hydrolytic acid solvent had a degradation effect on this polymer, corresponding to a general lowering of the peak degradation temperature in an oxidative atmosphere condition. The last step around 500-550 °C, corresponds to the final residues' degradation, and remained almost unaltered. The perceived behavior was found in all the compositions regardless the presence of PAni.

Given the lower thermo-oxidative stability of the scaffolds as a function of the dissolution time, hydrolytic degradation of the PCL fraction may have occurred. This perception will be subsequently assessed in the next sections.
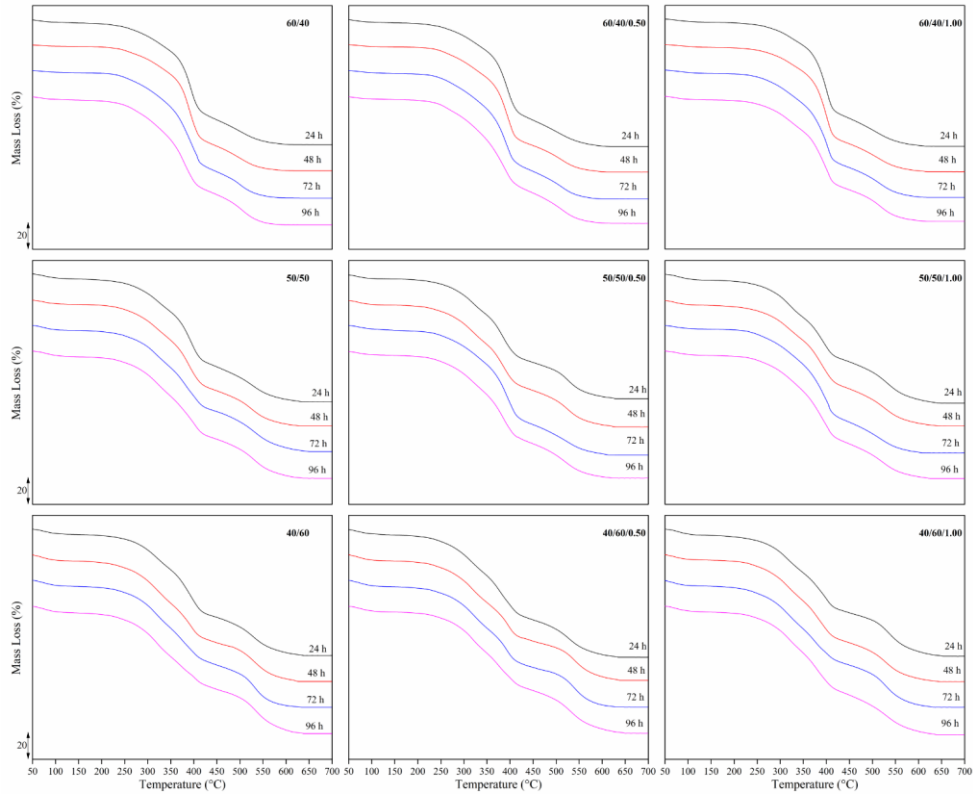
Fig. 25 Mass loss % curves of PCL/Ge/PAni scaffolds at different concentrations and dissolution time.
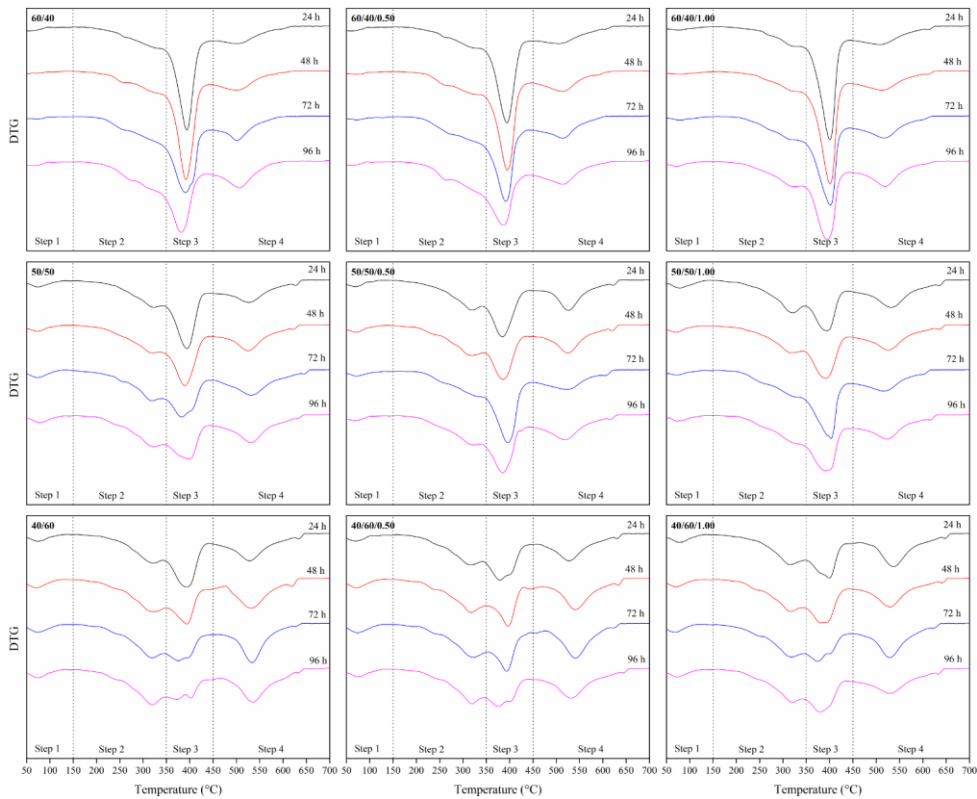
Fig. 26 DTG curves of PCL/Ge/PAni scaffolds at different concentrations and dissolution time.

Tab. 11 Peak temperatures for each degradation step for different concentration of PCL/Ge/PAni.

PCL/Ge (%)	PAni (%)	D.T. (h)	T_p (°C)			
			Step 1	Step 2	Step 3	Step 4
60/40	-	24	55.94	257.08	393.61	503.09
		48	44.87	253.55	392.33	500.22
		72	69.89	254.96	390.03	501.77
		96	66.92	270.53	381.96	506.92
	0.50	24	59.81	261.27	394.19	504.27
		48	72.02	259.15	396.64	514.02
		72	72.75	264.81	392.59	514.94
		96	46.00	265.5	385.77	514.94
	1.00	24	75.71	318.09	400.55	507.7
		48	79.18	317.89	400.77	518.11
		72	75.97	323.01	401.06	512.38
		96	71.83	315.98	392.40	518.87
50/50	-	24	74.73	323.57	393.91	527.23
		48	70.31	313.52	388.33	524.73
		72	72.72	318.98	382.23	531.05
		96	75.71	323.76	396.38	531.42
	0.50	24	69.06	320.01	384.06	527.12
		48	70.54	319.73	386.31	525.14
		72	73.36	327.59	398.23	523.06
		96	69.28	323.52	385.55	519.71
	1.00	24	79.37	321.38	394.06	531.03
		48	60.72	319.89	391.64	526.37
		72	70.87	321.23	403.62	501.77
		96	72.36	325.47	391.03	506.92
40/60	-	24	73.95	323.03	394.67	528.32
		48	72.24	320.98	392.97	531.06
		72	76.09	319.40	375.28	535.05
		96	73.36	320.51	371.21	536.43
	0.50	24	69.51	315.95	378.99	528.06
		48	73.57	316.29	396.52	541.47
		72	75.62	322.17	393.76	542.30
		96	74.50	319.64	376.08	533.36
	1.00	24	75.95	315.74	399.62	537.54
		48	71.65	316.18	381.04	528.97
		72	68.86	319.22	375.00	528.47
		96	73.23	320.47	379.19	529.57

G. Mezzasalma

4.3.3 *Thermal properties*

With the purpose of assessing the changes in the microstructure as a function of the dissolution time, the thermal properties were evaluated by means of differential scanning calorimetry (DSC). Fig. 28 and Fig. 29 plots the DSC thermograms of the heating, cooling scans for PCL/Ge/PAni scaffolds electrospun after 24, 48, 72 and 96 h of dissolution time in the hydrolytic acid solvent. Results of the peak temperatures with the corresponding enthalpies of the melting and crystallization are gathered in Tab. 12.

In the first heating scan the melting peak is placed at around 60 °C, ascribed to the typical PCL melting behavior, sharpened and moved towards lower temperatures with the increase of the dissolution time in the hydrolytic acid solvent. It can be correlated to a crystalline development of lower size as a function of the dissolution time.

During the cooling scan (Fig. 29), a crystallization transition occurred, at peak temperature (T_c) around 28 °C, showing an increase in their values for higher dissolution time.

Since the changes in the melting and crystallization are closely related to the change in the molar mass of a polymer given the higher chain mobility to crystallize, the perceived variations are in line with the decrease of the molar mass of the PCL fraction of the scaffolds as the dissolution time increased [48].

As observed in the previous subsection, the thermal behavior was similar in all the compositions regardless the presence of PAni.
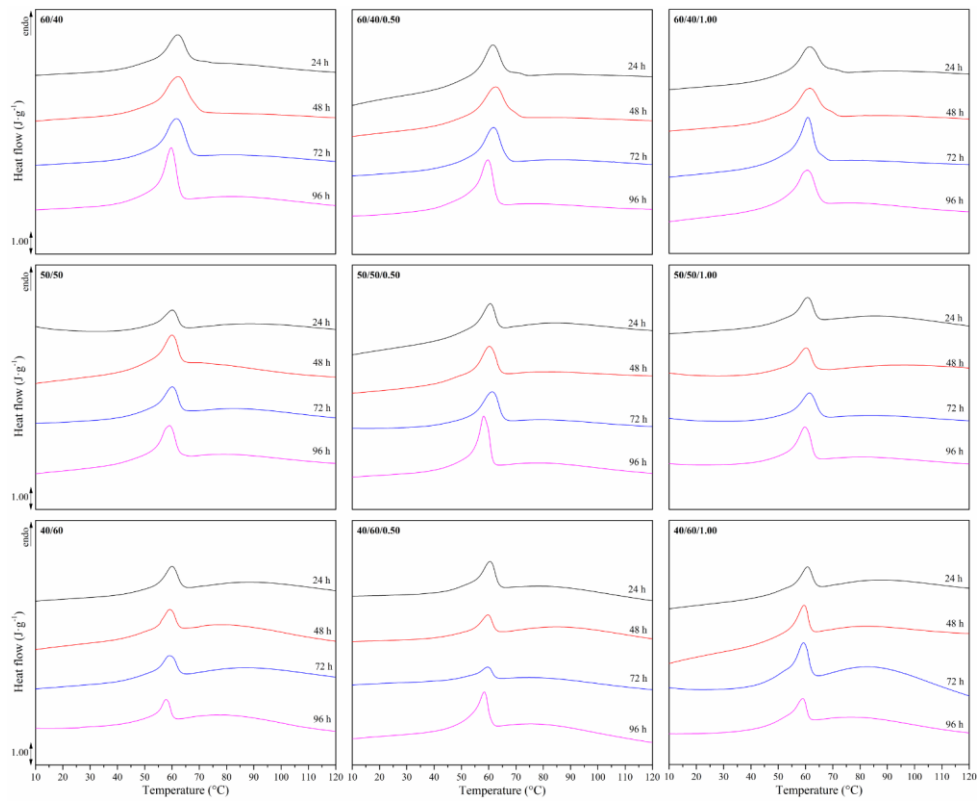
Fig. 27 DSC thermograms of the heating of PCL/Ge/PAni scaffolds at different concentrations and dissolution time.
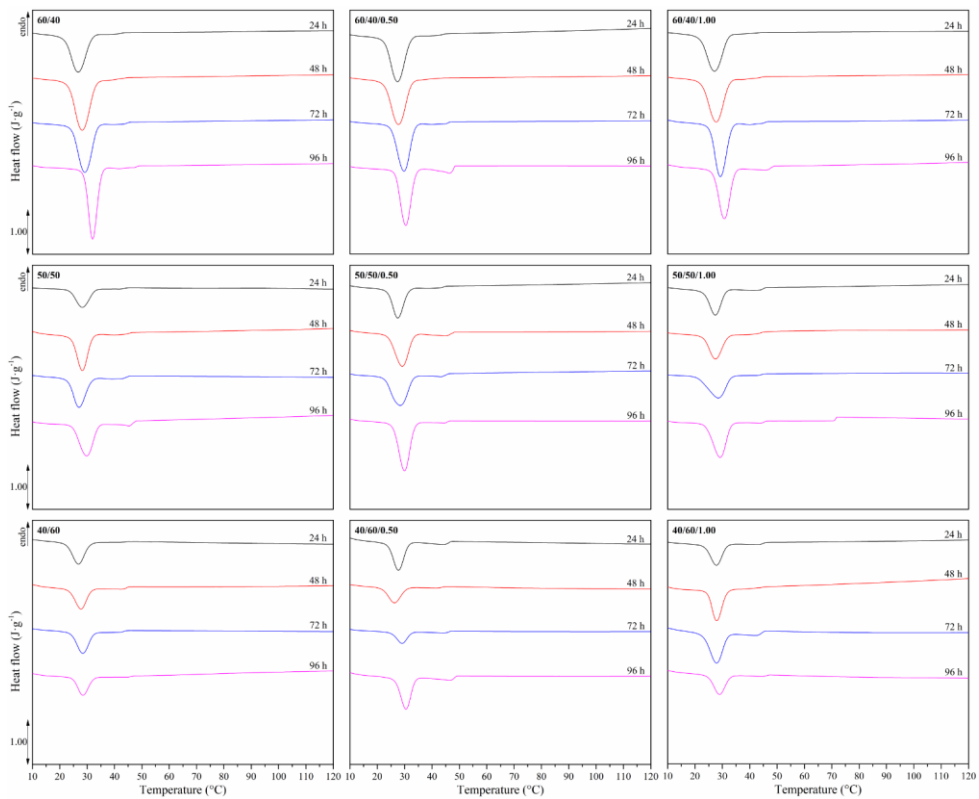
Fig. 28 DSC thermograms of the cooling of PCL/Ge/PAni scaffolds at different concentrations and dissolution time.

Tab. 12 Melting and crystallization enthalpies and corresponding temperatures.

PCL/Ge (%)	PAni (%)	D.T. (h)	Heating		Cooling	
			Δh_m (J/g)	T_m (°C)	Δh_c (J/g)	T_c (°C)
60/40	-	24	42.71	62.02	-15.86	26.91
		48	58.26	62.15	-14.06	27.71
		72	51.55	61.66	-15.79	28.41
		96	51.82	59.85	-12.11	28.34
	0.50	24	47.27	61.45	-18.02	27.72
		48	51.01	62.5	-7.38	29.06
		72	47.65	61.85	-15.58	26.2
		96	52.31	59.73	-25.52	30.39
	1.00	24	42.2	61.33	-17.02	27.73
		48	46.64	61.48	-21.95	27.89
		72	50.55	60.88	-29.69	27.9
		96	48.54	60.72	-16.58	29.03
50/50	-	24	19.69	59.91	-26.17	28.22
		48	32.17	59.9	-26.08	27.07
		72	30.11	59.06	-32.28	29.9
		96	37.23	59.91	-14.33	28.17
	0.50	24	24.58	60.38	-34.72	27.57
		48	29.57	60.23	-29.57	28.39
		72	33.71	61.27	-30.61	29.7
		96	40.22	58.17	-21.86	29.95
	1.00	24	23.35	60.54	-21.52	27.58
		48	23.75	60.16	-22.48	27.52
		72	28.38	61.49	-24.97	28.53
		96	32.73	59.77	-30.93	29.23
40/60	-	24	19.84	59.88	-35.75	26.78
		48	19.12	59.08	-47.19	28.32
		72	20.72	59.06	-42.52	29.14
		96	14.85	57.98	-43.47	31.97
	0.50	24	26.54	60.42	-38.99	27.49
		48	16.69	59.59	-38.02	27.8
		72	11.29	59.55	-39.28	29.8
		96	31.03	58.39	-45.63	30.26
	1.00	24	19.97	60.54	-35.99	27.13
		48	25.91	59.39	-43.75	27.83
		72	34.04	59.25	-41.86	29.27
		96	21.48	58.94	-42.36	30.75

4.3.3.1 Crystallinity degree of the PCL fraction

The crystallinity degree was evaluated using the Eq. 1, its evolution for the scaffolds is plotted in Fig. 30. There, the influence of the PCL and Ge concentration was clear: the X_c decreased as a function of the Ge concentration passing from $\approx$ 55 % of the 60/40 configurations to $\approx$ 35 % of the 40/60 configurations. The PAni still did not revealed any appreciable change.

The scaffolds with higher PCL content, the 60/40 and the 50/50 configurations, showed an increasing tendency of the X_c as a function of the dissolution time, this behavior could be as a consequence of the hydrolytic degradation of the PCL chains in which shorter macromolecular segments with enhanced mobility were more capable of forming crystalline domains than longer segments. These smaller segments may have promoted enhanced crystallization and orientation along the fiber axis [68].

However, the 40/60 PCL/Ge scaffolds showed a not clear behavior. As an example, for the 40/60 and 40/60/1.00 an increase in X_c until 72 h of dissolution time was found, then lower crystallinity degree was observed as the dissolution time increased. This could be explained with the fact that higher hydrolytic degradation of the PCL segments for these compositions seemed to result in too short PCL segments to develop substantial crystallization with the presumable diffusion of the PCL macromolecules into the Ge matrix, thus hindering the PCL crystallization [49].
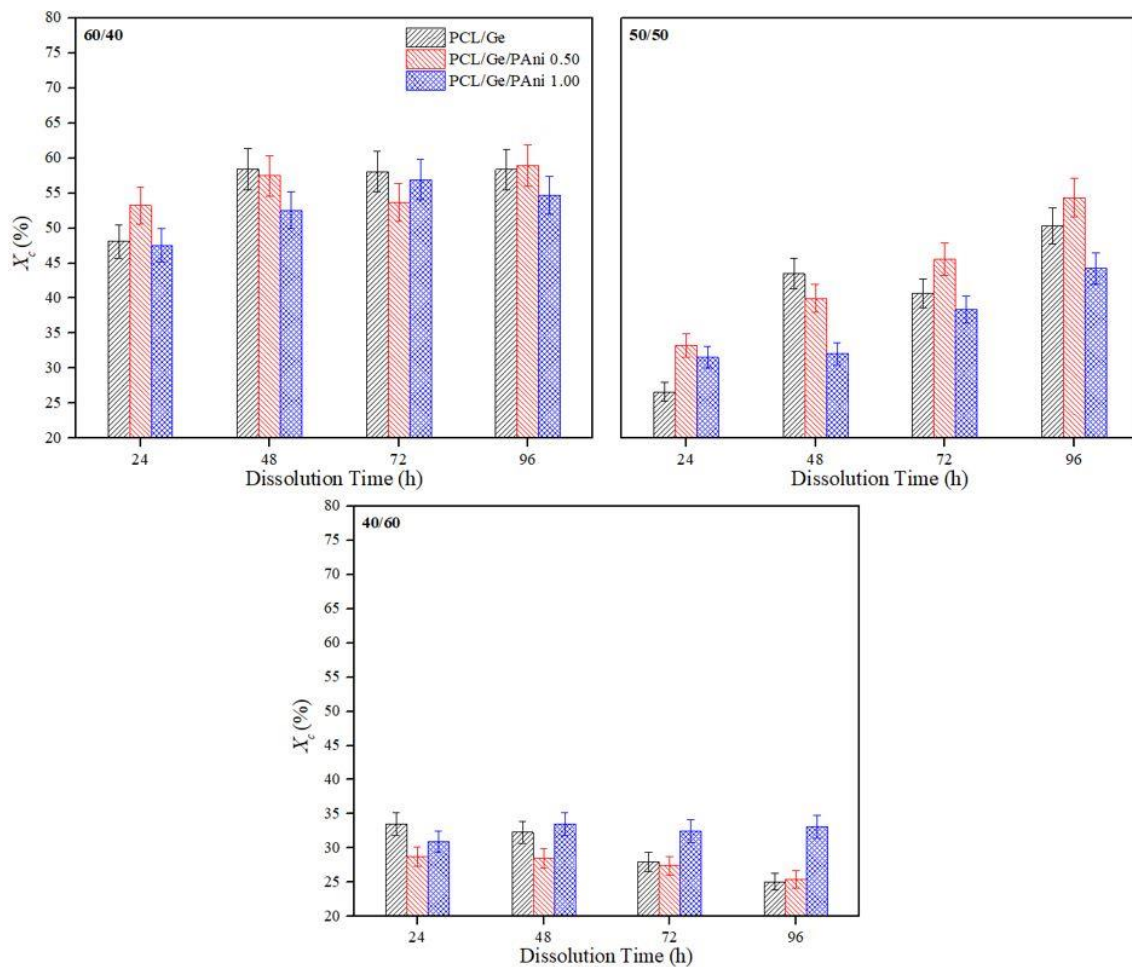
Fig. 30 Crystallinity degree of PCL/Ge/PAni scaffolds at different concentrations and dissolution time.

4.3.3.2 Lamellar thickness of the PCL fraction

Fig. 31 plots the evolution of the lamellar thickness (l_c), calculated by means of Eq. 2. As it is shown, while the PAni did not induced an appreciable influence, the increase in Ge showed a strong influence on the lamellar thickness decreasing it from ≈ 35 to ≈ 28 nm. Also, the dissolution time appeared to influence the l_c of the scaffold, showing a decrease from ≈ 35 nm to ≈ 31 nm for 60/40 configurations, from ≈ 31 nm to ≈ 28 nm for 50/50 and 40/60 configurations. This decrease as a function of the dissolution time can be associated to the lower PCL chain sizes, that resulted into a more imperfect crystallization, traduced in lower lamellar thickness, as hydrolytic degradation advanced during immersion into the acidic solvent.
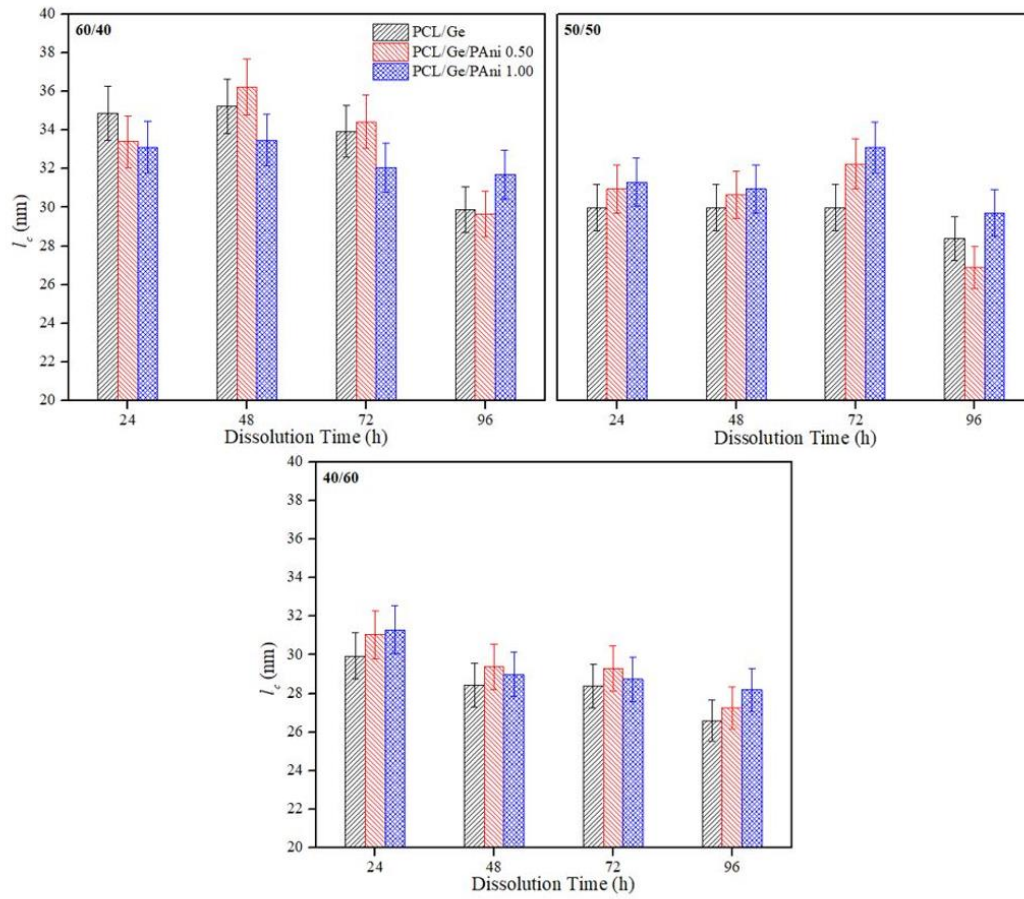
Fig. 29 Lamellar thickness of PCL/Ge/PAni scaffolds at different concentrations and dissolution time.

4.3.4 *Molar mass degradation of the PCL fraction*

The effect of dissolution time in the tailoring strategy was assessed also by means of molar mass analyses of the scaffolds through size exclusion chromatography (SEC). The molar mass was evaluated in terms of average molar mass in number (M_n), average molar mass in weight (M_w), polydispersity index (*PDI*), intrinsic viscosity (*IV*) and hydrodynamic radius (*Rh*) in THF. as shown in Fig. 33, Fig. 34 and Tab. 13 for the pellet of PCL and electrospun scaffolds as a function of dissolution time in the hydrolytic acid solvent.

As reported in Tab. 13, M_n decreased from 90140 to ≈12000 g·mol^{-1}, while M_w moved from 131400 to ≈21000 g·mol^{-1} from the raw PCL (pellet) to the scaffolds electrospun after 96 h in the acidic environment.

While Fig. 33 plots the average trend of M_n with the dissolution time, in Fig. 34 are shown the results of the SEC, plotting M_n distributions as a function of the dissolution time. When the dissolution time increased, a displacement of the molar mass distributions towards lower values was observed, due to hydrolytic degradation of the ester bond and subsequent chain scission [48]. The hydrolytic reaction may occur as a depolymerization process and random chain scission mechanism, highly catalyzed by the formic/acetic acid solution, which is frequently terminated by carboxylic acid end groups and hydroxyl end groups [69], as shown in Fig. 32.
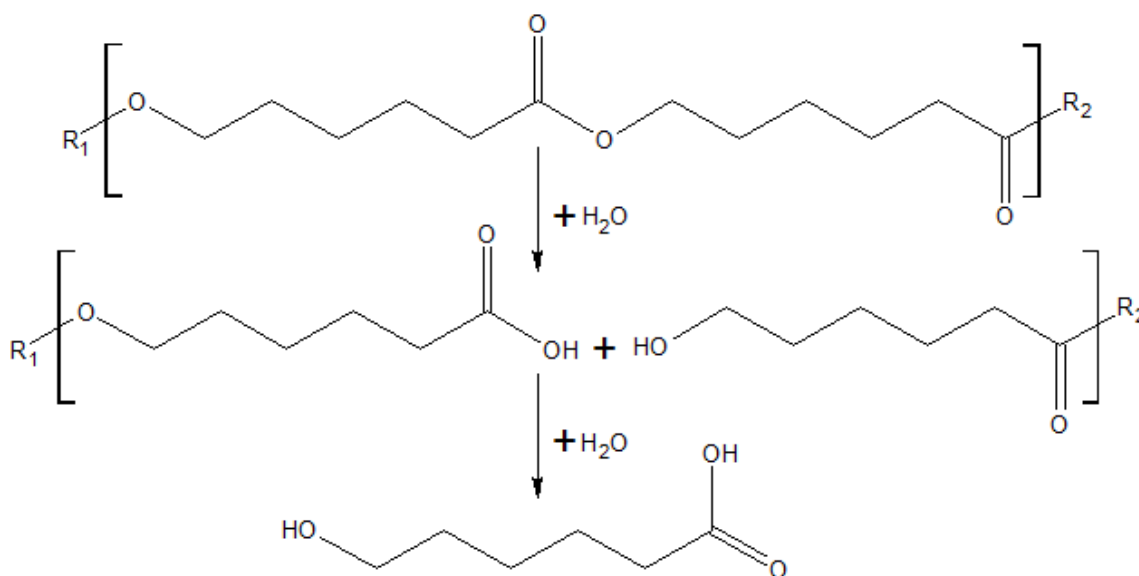
Fig. 32 Hydrolytic degradation scheme of the PCL [70].

As the dissolution time increased low molar mass peaks around 10 000 g·mol^{-1} started to appear, becoming more intense after 96 h. From Fig. 33 and considering only the 24 h data, it is possible to understand also that, moving from the 60/40 to the 40/60 configurations, the increase in the Ge concentration turn the single-peak distribution into a multi-peak distribution, this behavior, as reported in [71], is attributed to the emulsion of PCL into the Ge matrix diluted in the formic/acetic acid mixture.
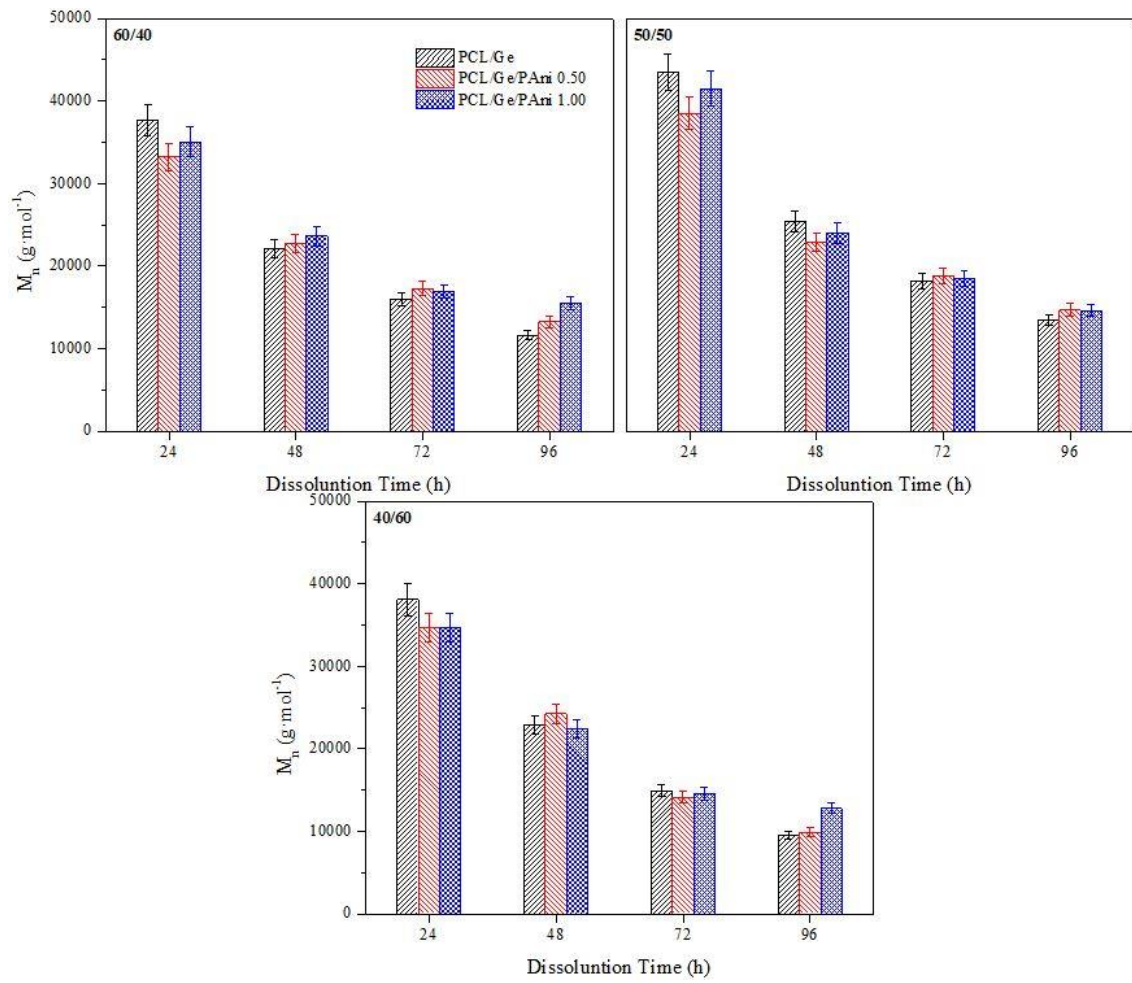
Fig. 33 Average molar mass in number as a function of the dissolution time

Fig. 34 Molar mass distribution as a function of the dissolution time.

Tab. 13 Average molar mass in number (M_n), average molar mass in weight (M_w), polydispersity index (PDI), intrinsic viscosity (IV) and hydrodynamic radius of PCL pellet and PCL/Ge/PAni scaffolds at different concentrations and dissolution time.

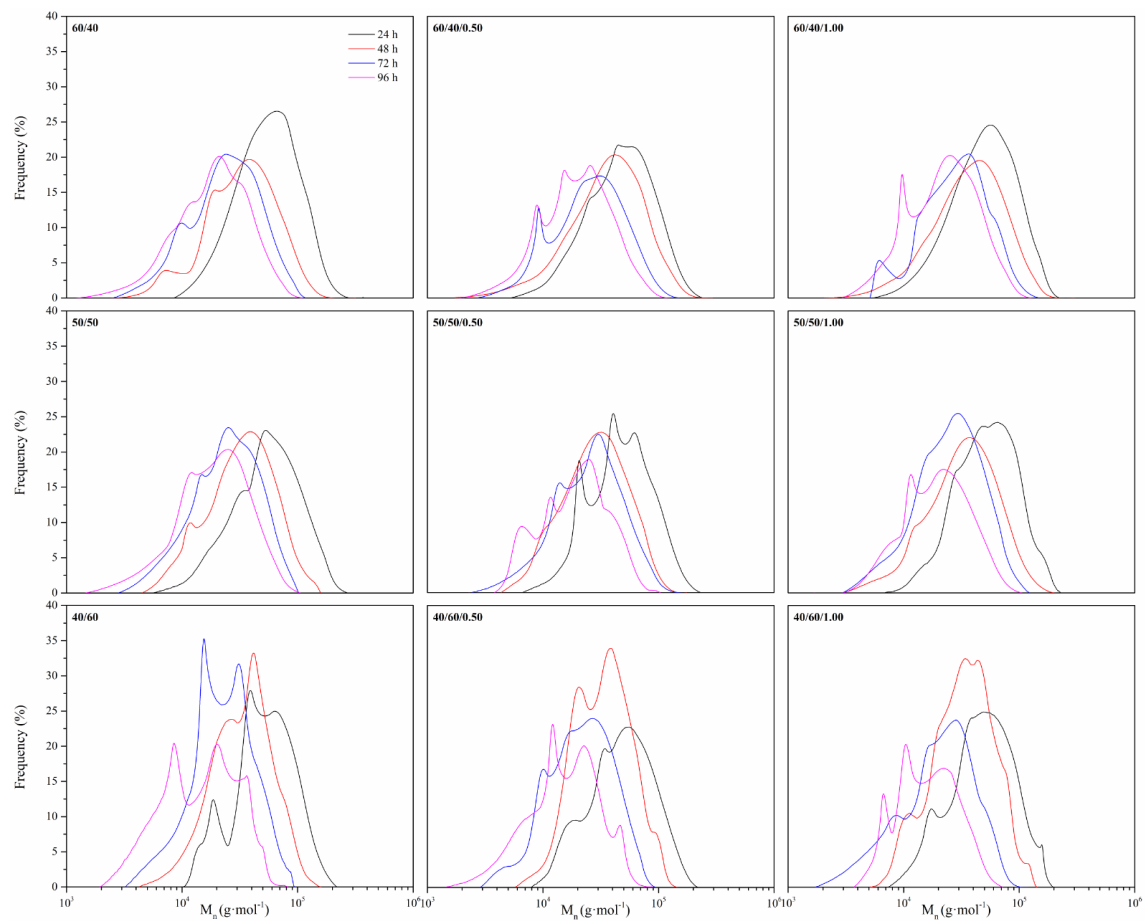| PCL/Ge (% wt.)	PAni (% wt.)	D.T. (h)	M_n (g·mol⁻¹)	M_w (g·mol⁻¹)	PDI	IV (dL·g⁻¹)	R_h (nm)
pellet	-	0	90140	131400	1.46	1.10	12.82
		24	37610	63410	1.69	0.62	8.23
	-	48	22120	39840	1.80	0.45	6.30
		72	16030	28840	1.80	0.36	5.23
		96	11620	22290	1.92	0.30	4.51
		24	33200	55790	1.68	0.56	7.63
60/40	0.50	48	22700	44180	1.95	0.48	6.65
		72	17240	30390	1.76	0.36	5.34
		96	13250	23590	1.78	0.30	4.65
		24	35070	58490	1.67	0.59	7.86
	1.00	48	23650	44360	1.88	0.48	6.66
		72	16930	32110	1.90	0.37	5.49
		96	15560	26760	1.72	0.33	4.99
		24	39150	64670	1.65	0.63	8.31
	-	48	22860	38860	1.70	0.43	6.18
		72	16370	28670	1.75	0.35	5.22
		96	12130	22870	1.89	0.30	4.58
		24	34670	55670	1.61	0.56	7.60
50/50	0.50	48	20610	33470	1.62	0.39	5.67
		72	16950	29920	1.76	0.35	5.29
		96	13220	22570	1.71	0.29	4.51
		24	37350	59920	1.60	0.58	7.89
	1.00	48	21590	39350	1.82	0.44	6.24
		72	16610	29060	1.75	0.35	5.24
		96	13120	23130	1.76	0.29	4.56
		24	38050	60250	1.58	0.59	7.95
	-	48	22900	37710	1.65	0.42	6.08
		72	14910	25340	1.70	0.32	4.83
		96	9520	17590	1.85	0.25	3.93
		24	34640	55810	1.61	0.56	7.62
40/60	0.50	48	24250	36970	1.53	0.42	6.08
		72	14110	24090	1.71	0.32	4.76
		96	9900	18530	1.87	0.26	4.05
		24	34650	56030	1.62	0.57	7.67
	1.00	48	22370	36810	1.65	0.42	6.01
		72	14560	23850	1.64	0.30	4.66
		96	12770	19060	1.49	0.26	4.13

4.3.4.1 Molar mass-loss model

In Fig. 35, it can be observed the correlation between the experimental data and theoretical curve of the M_n values as a function of time for the different PCL/Ge/PAni concentrations evaluated using the Eq. 4. The adapted model allows the prediction of M_n of PCL as a function of dissolution time. This model is very useful to predict and control the M_n and thus the fiber morphology, as demonstrated in Fig. 35 by the adaptation of the model curve with the experimental data.
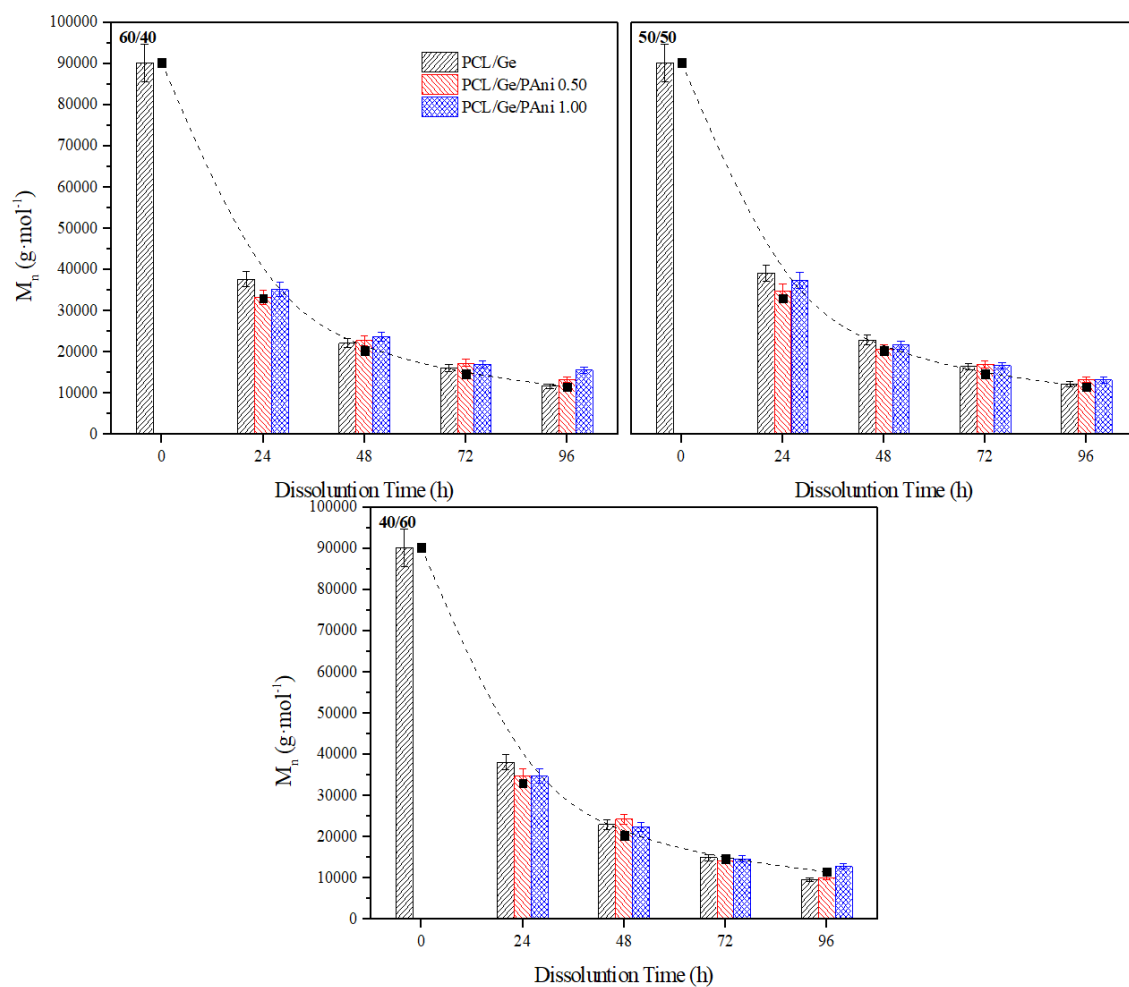

Fig. 35 Average molar mass in number as a function of the dissolution time with model.

4.4   Preliminary validation

The *in vitro* behavior of the electrospun PCL/Ge/PAni scaffolds was assessed by means of immersion in PBS, according to the international norm ISO 10993-13:2010-method 4.3 [62]. The validation procedure extent was established to 100 days, which was considered as a reasonable time-span to evaluate changes along their hypothetical service life.

The variations of the mass and the pH of the degradation media are plotted in Fig. 36. The effect of the variation of the Ge content in the scaffolds, influenced the scaffold mass loss process. In particular, an increase of the Ge concentration means an increase in the mass dissolved in the PBS media. Indeed, the mass loss can be directly correlated to the Ge release during immersion [72].

The presence of the PAni in the scaffolds, did not influenced the mass loss of the 60/40 and 50/50 PCL/Ge scaffolds. However, the 40/60 composition revealed higher mass loss as PAni content increased. These results must be deeply assessed in terms of other properties such as the molar mass variation in order to corroborate the effect of the PAni in the hydrolytic degradation of the scaffolds.

Considering the dissolution time, slightly higher mass loss was appreciated for all the three compositions electrospun after 24 h, 48 h and 72 h. A more pronounced loss was perceived for scaffolds with a dissolution time of 96 h. The scaffolds containing PAni electrospun after 96 h were not evaluated, given its difficult handling prior to immersion. The higher mass loss as dissolution time increased can be correlated to the liberation of low molar mass hydrolytically degraded PCL segments.

The evaluation of the pH of the PBS dissolution corroborated the slow degradation of the PCL molecules in simulated service conditions as well as the buffer ability to the feasible released PCL acid oligomers. In this sense, the pH remained around 7 for all the studied compositions after 100 days of immersion.
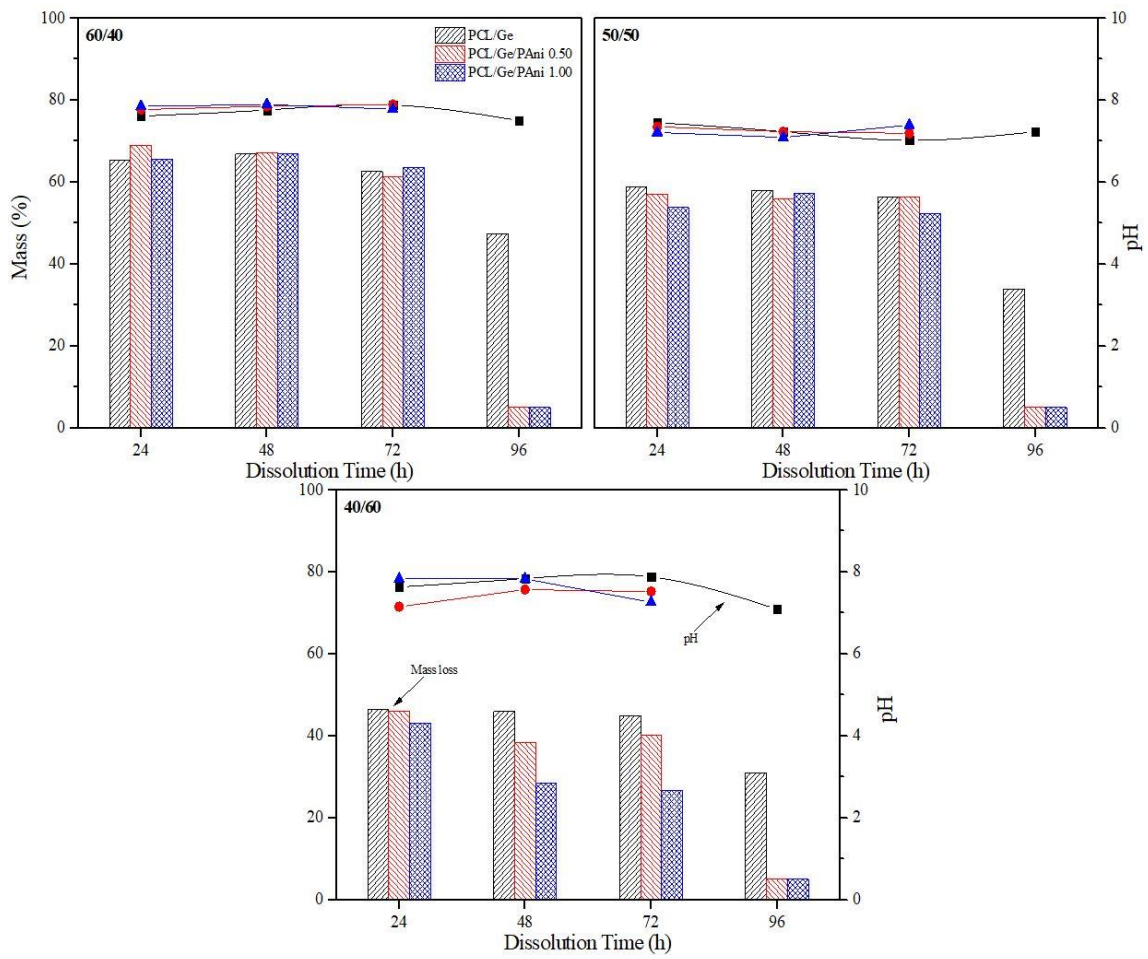
Fig. 36 Remaining mass and pH after 100 days of immersion in simulated service conditions (PBS) as a function of the composition and dissolution time.

5 Conclusions

Nanofibrous scaffolds were obtained by means of electrospinning of PCL/Ge/PAni at different proportions using 1:1 formic acid/acetic acid as solvent.

For scaffolds obtained after 24 h of dissolution, it was found that the morphology and also the physico-chemical properties of the scaffold, were influenced by the Ge concentration, while the PAni seemed to have no effects with the exception of bringing electric conductivity to the nanofibers.

The dissolution time in the hydrolytic acid solvent was found to play a key role in the resultant physico-chemical properties and morphology of the electrospun scaffolds. Bead-free fibers were obtained after 24 h and 48 h of dissolution time, while some beads appeared at higher dissolution time. The hydrolytic chain scission of the PCL fraction decreased the molar mass of the electrospun scaffolds, increased the crystallinity degree and reduced the lamellar thickness.

The preliminary *in vitro* validation of the scaffolds in simulated service conditions revealed that the combination of the PCL, Ge and PAni, along with the effect of the dissolution time in the acidic solution prior to electrospinning would allow to control the degradation behavior of the scaffolds. In particular, high concentration of PCL and low dissolution time scaffolds can be used for long term applications while higher Ge and PAni concentration together with high dissolution time resulted in a higher degradation of the scaffolds.

Future investigations will open up the possibility to increase the PAni concentration with the goal to increase the conductivity of the scaffolds, as well as assessing their behavior in terms of *in vitro* biocompatibility and further *in vivo* implantation.

G. Mezzasalma

6   References

[1]   N. Zhang and D. H. Kohn, "Using polymeric materials to control stem cell behavior for tissue regeneration," *Birth Defects Res. C Embryo Today 96*, pp. 63–81, 2012.

[2]   D. I. Braghirolli, D. Steffens, and P. Pranke, "Electrospinning for regenerative medicine: A review of the main topics," *Drug Discov. Today*, vol. 19, no. 6, pp. 743–753, 2014.

[3]   Y. Li *et al.*, "Enhanced adhesion and proliferation of human umbilical vein endothelial cells on conductive PANI-PCL fiber scaffold by electrical stimulation," *Mater. Sci. Eng. C*, vol. 72, pp. 106–112, 2017.

[4]   D. Li *et al.*, "A comparison of nanoscale and multiscale PCL/gelatin scaffolds prepared by disc-electrospinning," *Colloids Surfaces B Biointerfaces*, vol. 146, pp. 632–641, 2016.

[5]   A. Martins, R. L. Reis, and N. M. Neves, "Electrospinning: processing technique for tissue engineering scaffolding," *Int. Mater. Rev.*, vol. 53, no. 5, pp. 257–274, 2008.

[6]   A. Haider, S. Haider, and I. K. Kang, "A comprehensive review summarizing the effect of electrospinning parameters and potential applications of nanofibers in biomedical and biotechnology," *Arab. J. Chem.*, 2015.

[7]   J. Yong-Chao, J. Lin, H. An, W. Xiao-Feng, L. Qian, and T. Lih-Sheng, "Electrospun polycaprolactone/gelatin composites with enhanced cell–matrix interactions as blood vessel endothelial layer scaffolds," *Mater. Sci. Eng. C*, vol. 71, pp. 901–908, Feb. 2017.

[8]   Y. Wu, Y. X. Chen, D. Q. J. Yan, P. Dong, S. W. Sawyer, and P. Soman, "Fabrication of conductive gelatin methacrylate-polyaniline hydrogels," *Acta Biomater*, vol. 33, pp. 122–130, 2016.

[9]   P. Hitscherich, S.Wu, R. Gordan, L. H. Xie, T. Arinzeh, and E. J. Lee, "The effect of PVDF-TrFE scaffolds on stem cell derived cardiovascular cells,"

68

Biotechnol.Bioeng., vol. 113, pp. 1577–1585, 2016.

[10] J. Zhang *et al.*, "The aligned core-sheath nanofibers with electrical conductivity for neural tissue engineering," *J.Mater. Chem. B*, vol. 2, pp. 7945–7954, 2014.

[11] M. Y. Li *et al.*, "Electroactive and nanostructured polymers as scaffold materials for neuronal and cardiac tissue engineering," *Chin. J. Polym. Sci.*, vol. 25, pp. 331–339, 2007.

[12] D. Kai, S. Shy Liow, and X. Jun Loh, "Biodegradable polymers for electrospinning: Towards biomedical applications," *Mater. Sci. Eng. C*, vol. 45, pp. 659–670, Dec. 2014.

[13] J. X. Law, L. L. Liau, A. Saim, Y. Yang, and R. Idrus, "Electrospun Collagen Nanofibers and Their Applications in Skin Tissue Engineering," *Tissue Eng. Regen. Med.*, no. August, 2017.

[14] M. Bognitzki *et al.*, "Nanostructured fibers via electrospinning," *Adv. Mater*, vol. 13, pp. 70–72, 2001.

[15] L. Ghasemi-Mobarakeh, M. P. Prabhakaran, M. Morshed, M.-H. Nasr-Esfahani, and S. Ramakrishna, "Electrospun poly(ε-caprolactone)/gelatin nanofibrous scaffolds for nerve tissue engineering," *Biomaterials*, vol. 29, no. 34, pp. 4532–4539, Dec. 2008.

[16] R. A. Perez and G. Mestres, "Role of pore size and morphology in musculo-skeletal tissue regeneration," *Mater. Sci. Eng. C*, vol. 61, pp. 922–939, 2016.

[17] S. J. Hollister, "Porous scaffold design for tissue engineering," *Nat. Mater*, vol. 4, pp. 518–524, 2005.

[18] *Tissue Engineering: Roles,Materials, and Applications*. Nova Publishers, 2008.

[19] M. Skotak, S. Noriega, G. Larsen, and A. Subramanian, "Electrospun cross-linked gelatin fibers with controlled diameter: The effect of matrix stiffness on proliferative and biosynthetic activity of chondrocytes cultured in vitro," *J. Biomed. Mater. Res. - Part A*, vol. 95, no. 3 A, pp. 828–836, 2010.

[20]   M. Kitsara, O. Agbulut, D. Kontziampasis, Y. Chen, and P. Menasché, "Fibers for hearts: A critical review on electrospinning for cardiac tissue engineering," *Acta Biomater.*, vol. 48, pp. 20–40, 2017.

[21]   J. Koleske, "Blends containing poly(e-caprolactone) and related polymers." In: Paul D, Newman S, editors. Polymer blends., New York: Academic Press Inc., pp. 369–389, 1978.

[22]   J. Gunn and M. Zhang, "Trends Biotechnol.," vol. 28, pp. 189–197, 2010.

[23]   G. Jin, M. P. Prabhakaran, D. Kai, S. K. Annamalai, K. D. Arunachalam, and S. Ramakrishna, "Tissue engineered plant extracts as nanofibrous wound dressing," *Biomaterials*, vol. 34, no. 3, pp. 724–734, 2013.

[24]   M. Ngiam *et al.*, "Tissue Eng.," vol. A 15, pp. 535–546, 2009.

[25]   S. Y. Chew, R. Mi, A. Hoke, and K. W. Leong, "Aligned protein-polymer composite fibers enhance nerve regeneration: A potential tissue-engineering platform," *Adv. Funct. Mater.*, vol. 17, no. 8, pp. 1288–1296, 2007.

[26]   M. P. Ghasemi-Mobarakeh, L. Prabhakaran, M. Morshed, M. H. Nasr-Esfahani, and S. Ramakrishna, "Electrical stimulation of nervecells using conductive nanofibrous scaffolds for nerve tissue engineering," *Tissue Eng.*, vol. A 15, pp. 3605–3619, 2009.

[27]   M. P. Prabhakaran, L. Ghasemi-Mobarakeh, G. Jin, and S. Ramakrishna, "Electrospun conducting polymer nanofibers and electrical stimulation of nerve stem cells," *J. Biosci. Bioeng.*, vol. 112, pp. 501–507, 2011.

[28]   E. Dolgin, "Taking tissue engineering to heart ;17:1032–5.," *Nat. Med.*, vol. 17, pp. 1032–1035, 2011.

[29]   F. Wang and J. Guan Jianjun, "Cellular cardiomyoplasty and cardiac tissue engineering for myocardial therapy," *Adv. Drug Deliv. Rev.*, vol. 62, no. 7–8, pp. 784–797, 2010.

[30]   N. Bhardwaj and S. C. Kundu, "Electrospinning: A fascinating fiber fabrication technique," *Biotechnol. Adv.*, vol. 28, no. 3, pp. 325–347, 2010.

[31]   M. P. Pavlov, J. F. Mano, N. M. Neves, and R. L. Reis, "Fibers and 3D mesh scaffolds from biodegradable starch-based blends: Production and characterization," *Macromol. Biosci.*, vol. 4, no. 8, pp. 776–784, 2004.

[32]   D. Zeugolis *et al.*, "Electro-spinning of pure collagen nano-fibres just an expensive way to make gelatin?," *Biomaterials*, vol. 29, pp. 2293–2305, 2008.

[33]   M. Hakkarainen, "Aliphatic polyesters abiotic and biotic degradation and degradation products," *Adv Polym Sci*, vol. 157, pp. 113–138, 2002.

[34]   S. R. Gomes *et al.*, "In vitro and in vivo evaluation of electrospun nano fi bers of PCL , chitosan and gelatin : A comparative study," vol. 46, pp. 348–358, 2015.

[35]   I. Rajzer, M. Rom, E. Menaszek, and P. Pasierb, "Conductive PANI patterns on electrospun PCL/gelatin scaffolds modified with bioactive particles for bone tissue engineering," *Mater. Lett.*, vol. 138, pp. 60–63, 2015.

[36]   M. A. Woodruff and D. W. Hutmacher, "The return of a forgotten polymer - Polycaprolactone in the 21st century," *Prog. Polym. Sci.*, vol. 35, no. 10, pp. 1217–1256, 2010.

[37]   A. C. Gurlek, B. Sevinc, E. Bayrak, and C. Erisken, "Synthesis and characterization of polycaprolactone for anterior cruciate ligament regeneration," *Mater. Sci. Eng. C*, vol. 71, pp. 820–826, 2017.

[38]   P. Aramwit, N. Jaichawa, J. Ratanavaraporn, and T. Srichana, "A comparative study of type A and type B gelatin nanoparticles as the controlled release carriers for different model compounds," *Mater. Express*, vol. 5, no. 3, pp. 241–248, 2015.

[39]   A. O. Elzoghby, "Gelatin-based nanoparticles as drug and gene delivery systems: Reviewing three decades of research," *J. Control. Release*, vol. 172, no. 3, pp. 1075–1091, 2013.

[40]   K. A. Ibrahim, "Synthesis and characterization of polyaniline and poly(aniline-co-o-nitroaniline) using vibrational spectroscopy," *Arab. J. Chem.*, vol. 10, pp. S2668–S2674, 2017.

[41]   J. C. C. Wu *et al.*, "Nanostructured bioactive material based on polycaprolactone

and polyaniline fiber-scaffolds," *Synth. Met.*, vol. 198, pp. 41–50, 2014.

[42] R. C. Dutta, M. Dey, A. K. Dutta, and B. Basu, "Competent Processing Techniques for Scaffolds in Tissue Engineering," *Biotechnol. Adv.*, 2017.

[43] J. M. Sobral, S. G. Caridade, R. A. Sousa, R. F. Mano, and R. L. Reis, "Three-dimensional plotted scaffolds with controlled pore size gradients: Effect of scaffold geometry on mechanical performance and cell seeding efficiency," *Acta Biomater.*, vol. 7, pp. 1009–1018, 2011.

[44] H. D. Lu, M. B. Charati, I. L. Kim, and J. A. Burdick, "Injectable shear-thinning hydrogels engineered with a self-assembling Dock-and-Lock mechanism," *Biomaterials.*, vol. 33, pp. 2145–2153, 2012.

[45] Z. Luo and S. Zhang, "Designer nanomaterials using chiral self-assembling peptide systems and their emerging benefit for society," *Chem. Soc.*, vol. 41, pp. 4736–4754, 2012.

[46] T. J. Sill and H. A. von Recum, "Electrospinning: Applications in drug delivery and tissue engineering," *Biomaterials*, vol. 29, no. 13, pp. 1989–2006, 2008.

[47] N. Lavielle *et al.*, "Controlled formation of poly(e-caprolactone) ultrathin electrospun nanofibers in a hydrolytic degradation-assisted process," 2013.

[48] O. Gil-Castell, J. D. D. Badia, E. Strömberg, S. Karlsson, and A. Ribes-Greus, "Effect of the dissolution time into an acid hydrolytic solvent to tailor electrospun nanofibrous polycaprolactone scaffolds," *Eur. Polym. J.*, vol. 87, pp. 174–187, 2017.

[49] O. Gil-Castell, J. D. Badia, and A. Ribes-Greus, "Tailored electrospun nanofibrous polycaprolactone/gelatin scaffolds into an acid hydrolytic solvent system," *Eur. Polym. J.*, vol. 101, no. February, pp. 273–281, 2018.

[50] V. Guarino, V. Cirillo, P. Taddei, M. A. Alvarez-Perez, and L. Ambrosio, "Tuning Size Scale and Crystallinity of PCL Electrospun Fibres via Solvent Permittivity to Address hMSC Response," *Macromol. Biosci.*, vol. 11, no. 12, pp. 1694–1705, Dec. 2011.

[51]   J. E. Mark, *Properties of Polymers Handbook*. Springer, 2007.

[52]   J. L. Lauritzen and J. D. Hoffman, "Theory of formation of polymer crystals with folded chains in dilute solution," *J. Res. Nat. Bur. Stand. 64*, pp. 73–102, 1960.

[53]   J. L. Lauritzen and J. D. Hoffman, "Crystallization of bulk polymers with chain folding theory of growth of lamellar spherulites," *J. Res. Nat. Bur. Stand.65*, pp. 297–336, 1961.

[54]   J. D. Hoffman, G. T. Davis, J. L. Lauritzen, and in N. B. H. (Ed.), "Crystalline and Noncrystalline Solids," New York, 1976.

[55]   O. Gil-Castell, J. D. Badia, R. Teruel-Juanes, I. Rodriguez, F. Meseguer, and A. Ribes-Greus, "Novel silicon microparticles to improve sunlight stability of raw polypropylene," *Eur. Polym. J. 70*, pp. 247–261, 2015.

[56]   Y. Suzuki, H. Duran, W. Akram, M. Steinhart, G. Floudas, and H. J. Butt, "Multiple nucleation events and local dynamics of poly(e-caprolactone) (PCL) confined to nanoporous alumina," *Soft Matter 9*, pp. 9189–9198, 2013.

[57]   C. Pitt and Z. Gu, "Modification of the rates of chain cleavage of poly(ε-caprolactone) and related polyesters in the solid state," *J Control Release*, vol. 4, pp. 283–292, 1987.

[58]   S. Lyu, R. Sparer, and D. Untereker, "Analytical Solutions to Mathematical Models of the Surface," no. March, pp. 383–397, 2004.

[59]   R. Simha, "Kinetics of degradation and size distribution of long Chain polymers," *J Appl Phys*, vol. 12(7), pp. 569–78, 1941.

[60]   N. Lavielle *et al.*, "Controlled formation of poly(ε-caprolactone) ultrathin electrospun nanofibers in a hydrolytic degradation-assisted process," *Eur. Polym. J.*, vol. 49, no. 6, pp. 1331–1336, 2013.

[61]   J. M. Flores, R. D. Romero, and J. G. Llongueras, "Espectroscopía de Impedancia Electroquímica en Corrosión," *Inst. Mex. Pet.*, p. 33, 2002.

[62]   ISO10993-13, "Biological evaluation of medical devices – Part 13: Identification

and quantification of degradation products from polymeric medical devices." 2010.

[63] S. Gautam, C. C. Amit, and K. Dinda, "Fabrication and characterization of PCL / gelatin / chitosan ternary nanofibrous composite scaffold for tissue engineering applications," *J. Mater. Sci.*, vol. 49, pp. 1076–1089, 2014.

[64] S.Amadori, P. Torricelli, K. Rubini, M. Fini, S. Panzavolta, and A. Bigi, "Effect of sterilization and crosslinking on gelatin films," 2015.

[65] M. Heidari, H. Bahrami, and M. Ranjbar-mohammadi, "Fabrication , optimization and characterization of electrospun poly (caprolactone)/ gelatin / graphene nano fi brous mats," vol. 78, pp. 218–229, 2017.

[66] S. Khorshidi and A. Karkhaneh, "Electrically conductive gel / fi bers composite scaffold with graded properties," *Mater. Sci. Eng. C*, vol. 74, pp. 238–245, 2017.

[67] H. Fong, I. Chun, and D. H. Reneker, "Beaded nanofibers formed during electrospinning," 2016.

[68] X. Wang, H. Zhao, L. S. Turng, and Q. Li, "Crystalline morphology of electrospun poly(e-caprolactone) (PCL) nanofibers," *Ind. Eng. Chem. Res.*, vol. 52, no. 13, pp. 4939–4949, 2013.

[69] R. Muthuraj, M. Misra, and A. K. Mohanty, "Hydrolytic degradation of biodegradable polyesters under simulated environmental conditions," *J. Appl. Polym. Sci.*, vol. 132, no. 27, p. n/a-n/a, Jul. 2015.

[70] S. Sandra, N. Diban, and A. Urtiaga, "Hydrolytic Degradation and Mechanical Stability of Poly (ε -Caprolactone)/ Reduced Graphene Oxide Membranes as Scaffolds for In Vitro Neural Tissue Regeneration," 2018.

[71] P. Denis, J. Dulnik, and P. Sajkiewicz, "Electrospinning and Structure of Bicomponent Polycaprolactone/Gelatin Nanofibers Obtained Using Alternative Solvent System," *Int. J. Polym. Mater. Polym. Biomater.*, vol. 64, no. 7, pp. 354–364, 2014.

[72] Q. Jiang, H. Xu, S. Cai, and Y. Yang, "Ultrafine fibrous gelatin scaffolds with deep

cell infiltration mimicking 3D ECMs for soft tissue repair," *J. Mater. Sci. Mater. Med.*, vol. 25, no. 7, pp. 1789–1800, Jul. 2014.